INQUA International Summer School
on Active Tectonics and Tectonic Geomorphology
24-27 September 2019, Prague

TERPRO commission

International Focus Group:
Earthquake Geology and
Seismic Hazards

CZECH
ASSOCIATION OF
GEOMORPHOLOGISTS

Field Trip Guide

26-27 September 2019

Flašar J. (ed.), Coubal M., Hartvich F., Burda J., Fischer T., Štěpančíková P., Tábořík P.

Field trip overview map

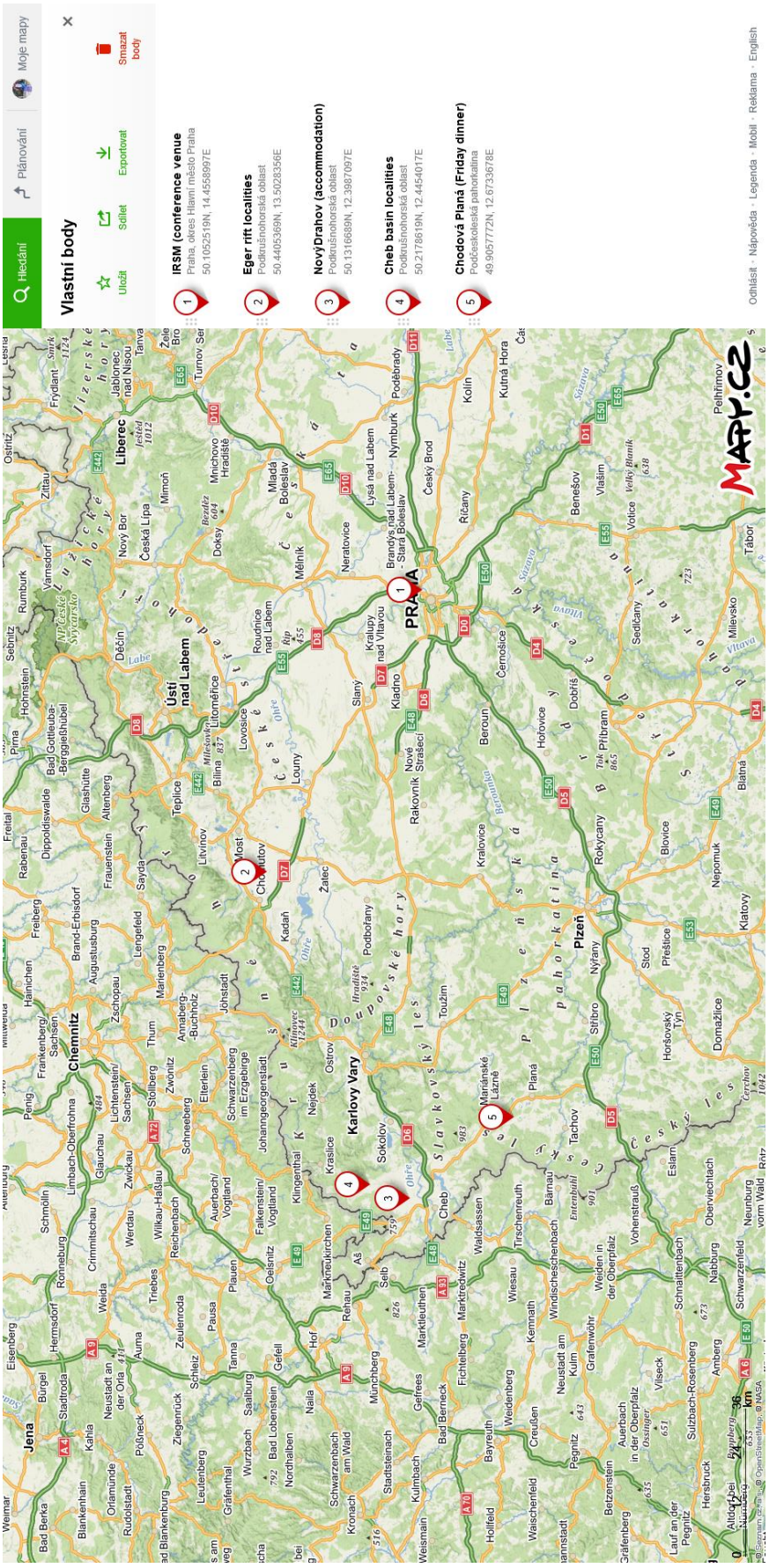

Thursday 26th September

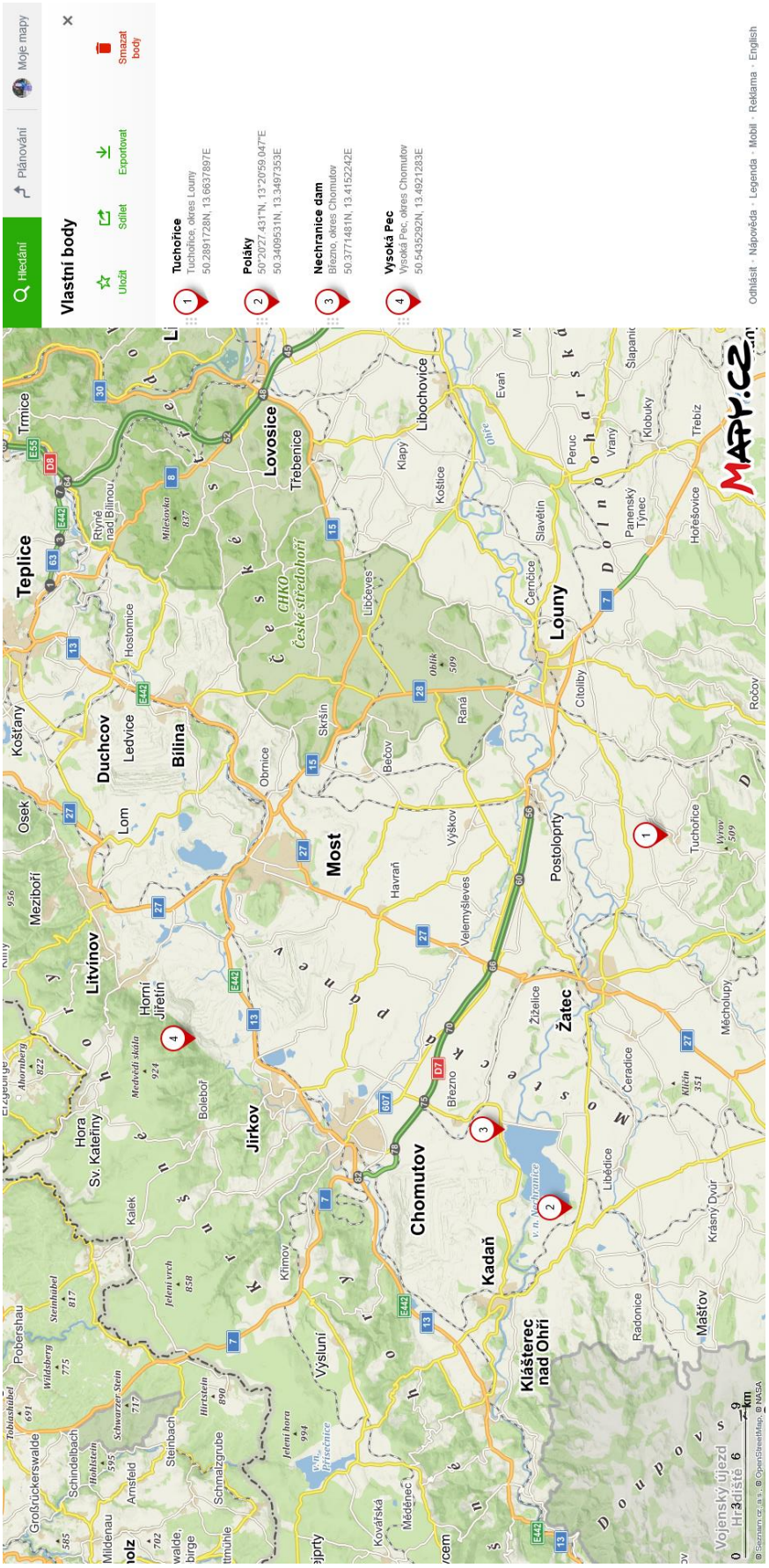

Friday 27th September

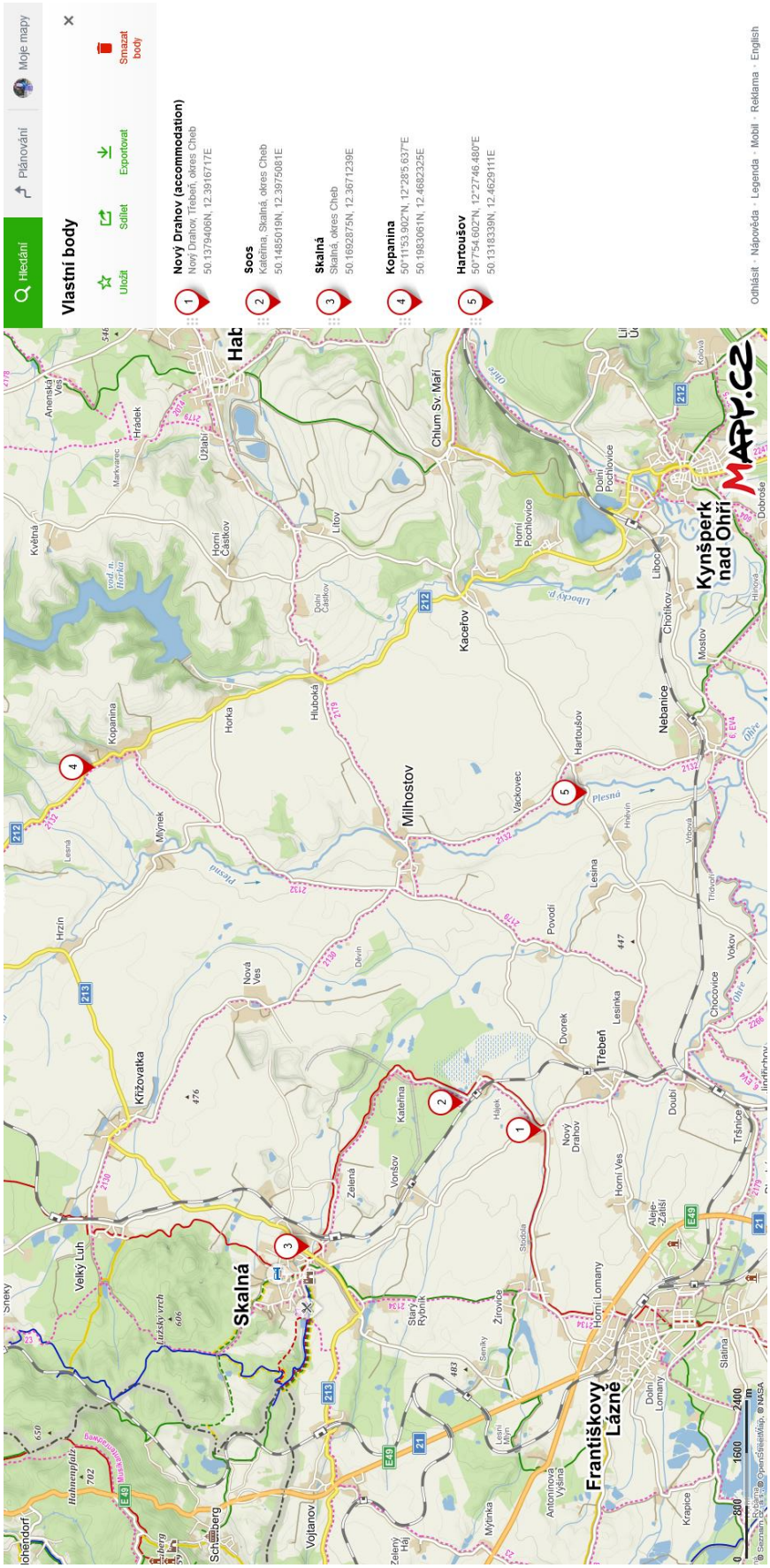

Field Trip Programme:

Thursday 26th September 2019

Departure: IRSM Prague, conference venue

1a) Introduction to the Eger Rift
(Coubal, M.)
1b) Tuchořice: southern marginal fault, slickensides and their measurement
(Coubal, M.)
2a) Poláky - Hořenická (Erdbrandová) rokle: fluvial sediments embedded into the fault zone, paleostress analysis of the slickenside planes
(Coubal, M.)
2b) Poláky: landslide
(Hartvich F.)
3a) Nechranice dam: outcrop of the central rift fault (Střezov fault)
(Coubal, M.)
3b) Nechranice dam: Slumps and rockfalls+ UAV remote sensing demonstration
(Hartvich. F.)
4) Vysoká Pec: Landslides along the foot of the Krušné Hory Mts.
(Hartvich F., Burda, J.)

Accommodation: Nový Drahov

Friday 27th September 2019

1) Introduction to the Cheb Basin
2) Soos
3a) Skalná: Geodynamic observatory and seismic station in Skalná
(Fischer, T.)
3b) Skalná: Fault monitoring using TM-71 3D dilatometer
(Hartvich, F.)
4a) Kopanina – Paleoseismic trenching site (backfilled trenches results)
(Štěpančíková, P.)
4b) Kopanina ERT and DEMP measurement method
(*Tábořík, P.)*
5)Hartoušov and Bublák moffette field
(Fischer, T.)
Dinner: Chodová Planá

Return to IRSM Prague, conference venue

Thursday 26th September

1a) Introduction to the Eger Rift

Origin of the Eger Rift

The Eger Rift is the deep-based volcanic/tectonic structure in the northern part of Bohemian Massif, which has been formed in several phases. There have been a discussion, whether the Eger Rift is or is not the real continental rift, however Kopecký (1971) described the structure as a proper rift and today, the Eger Rift is generally accepted as a part of the European Cenozoic Rift System – ECRIS (Dezés et al., 2004).

The rift itself is founded on the deep Litoměřice Fault, which formed a boundary between two zones of Variscan orogeny - the Teplá-Barrandian unit and Saxo-Thuringian unit. The complex volcanic-tectonic structure of the Eger rift has been formed in several phases during the Cenozoic reactivation of the Litoměřice fault. We can found a features, which are typical for a continental rifts: asymmetric graben, one-sided uplift of a bounding block, axial horst structure, higher heat flow, presence of an alkaline volcanism, negative gravimetric anomaly etc.

Volcanic Activity

The volcanism was active since 80 Ma (upper Cretaceous) till 0,5 Ma (Pleistocene) in the Eger Rift. There were a several phases of activity, with the maximum during the Oligocene epoch. Kopecký (1978) have set 4 phases of the volcanic activity:

I. (Upper Cretaceous – Paleogene): Nephelinite-Polzenite magma formed dykes in peripheral parts of the rift, orientation of dykes did not follow the main orientation of the rift

II. (Upper Eocene – middle Miocene): Volcanism of both phonolitic and basaltic chemism. In the beginning of the phase, huge accumulations of pyroclastics were formed (Střezov formation - Oligocene), the numerous bodies of intrusive volcanics can be found in a central horst of a the rift, some of them along the rift itself

III. (Upper Pliocene – lower Pleistocene): Lower activity than in previous phases. Subaerial lava flows or shallow subsurface intrusive bodies of basaltic lavas can be found in the peripheral parts of the rift (Plzeň, Turnov).

IV. (Pleistocene): Ultrabasic volcanism (mellilitic basalts) in the Cheb Basin (and far from the rift in Bruntál area).

Tectonic structure of the Eger rift

The **central horst** can be found in the inferior part of the Eger Rift. It forms a belt of uplifted blocks and megaanticlinal structures (Střezov ridge, Bílina elevation, České Středohoří Horst), where the older rocks (crystalline, cretaceous) can be found. In the southern part of the horst, we can see the **central rift fault** (Střezov fault), the northern part of the horst is formed by faults as well (Bílina Fault).

The **northern trough** (Choumtov Basin) is lying along the central horst on the northern side, on the southern side there is the **southern trough** (Žatec Basin). Both of the troughs are

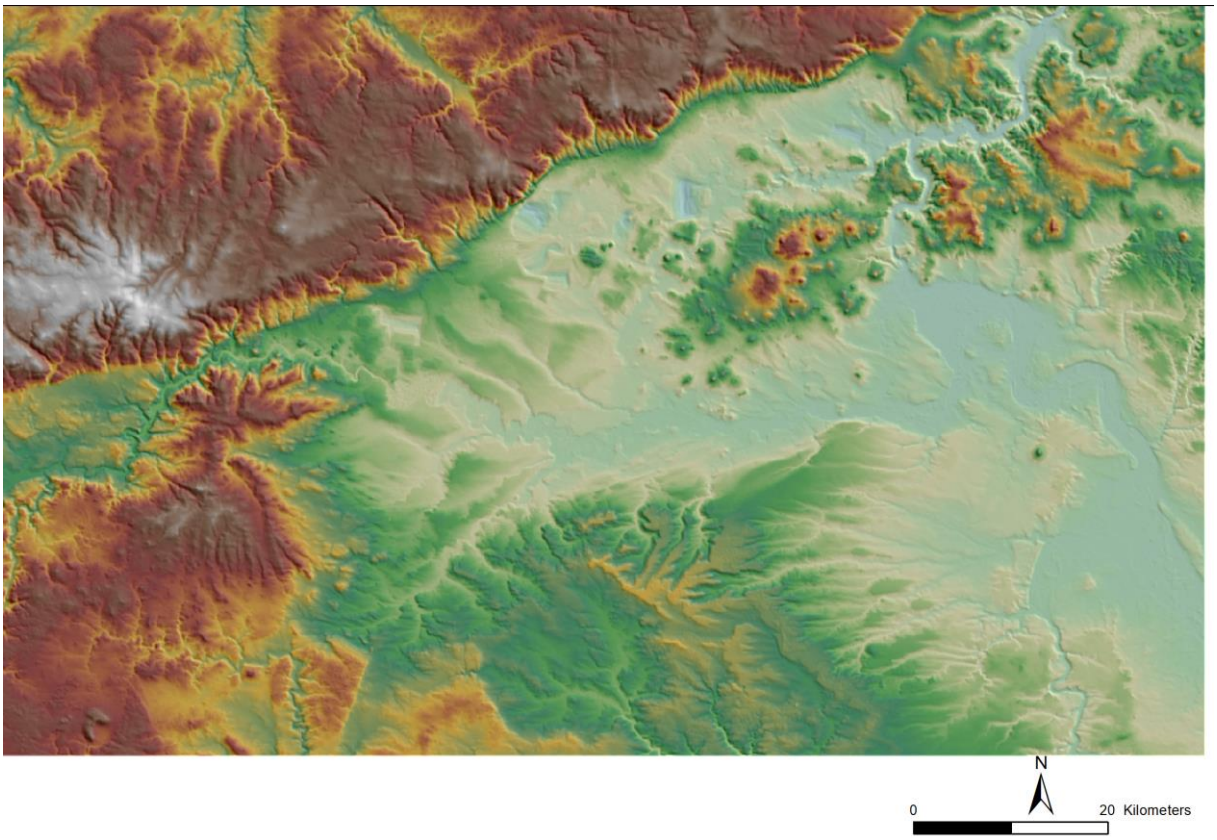

Fig. 1: Digital Elevation Model of the Eger Rift

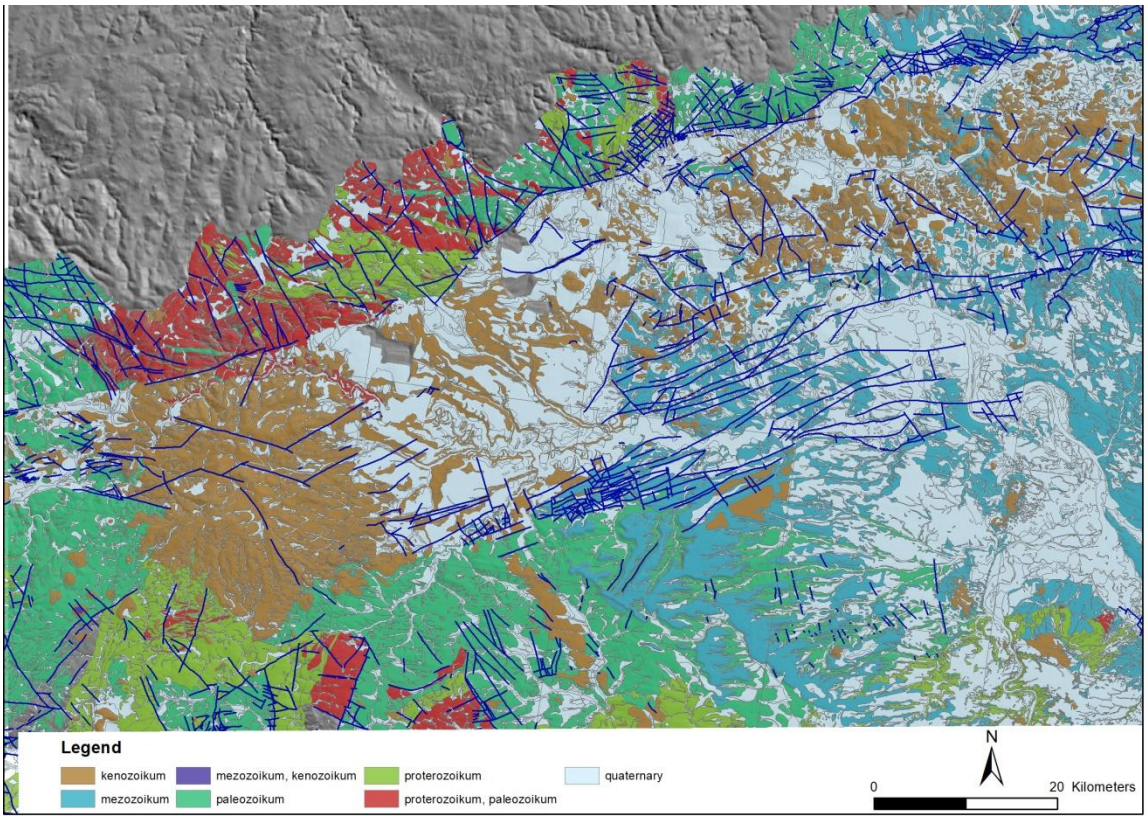

Fig. 2: Simplified geological map of the Eger Rift

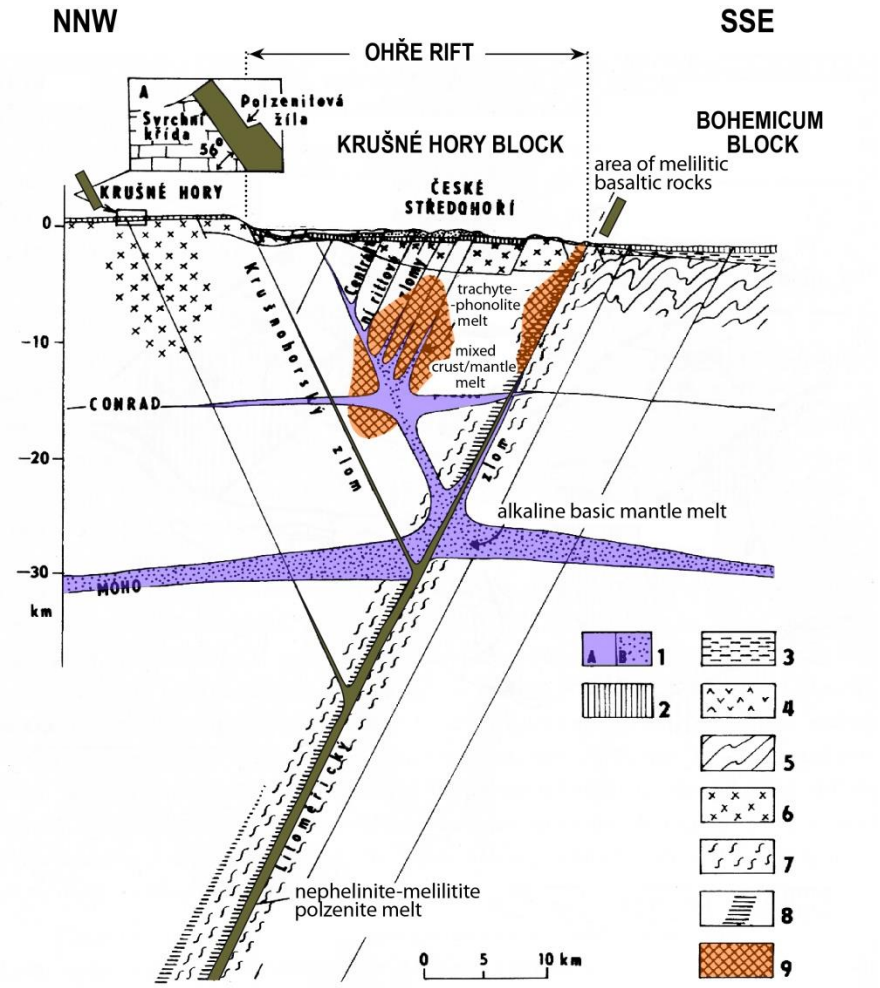

Fig. 3: A scheme of the deep-seated volcano-tectonic structure of the Ohře Rift (Kopecký 1987).

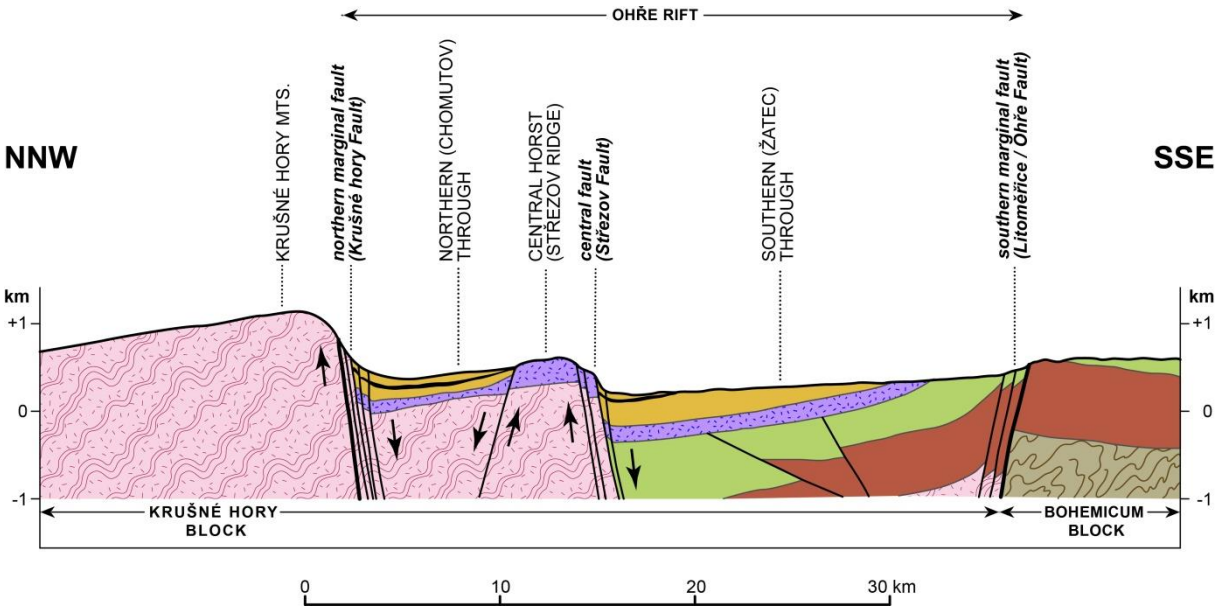

Fig. 4: Essential structural elements of near-surface portions of the Ohře Rift (adapted from from Kopecký, 1987).

filled with the Tertiary sediments – lower Střezov formation of volcanic-sedimentary origin (Oligocene) and upper Most formation (Miocene).
The rift is bounded by marginal faults. ***Southern marginal rift fault*** (Litoměřice/ Ohře Fault) is the surface outcrop of the deep Litoměřice Fault, which had been the original forming structure of the whole rift. The fault is composed from the wide zone of parallel faults or by constituent faults in en echelon setting. The central part of the rift is dropped by 200 m along the southern fault.
Northern marginal rift fault (Krušné hory Fault) was also reactivated in several phases; it has a simple structure of a normal fault. Characteristic feature of the fault is the massive normal fault drag of Miocene sediments from a foot-wall, which can be seen in an open-pit coal mines. After the end of a rift formation – Pliocene/Pleistocene, the block of Krušné hory Mts. was uplifted along this fault with a drop over 700 m.

1b) Tuchořice: southern marginal fault, slickensides and their measurement *(Coubal, M.)*

The locality is nearby the southern marginal fault (Ohře Fault) of the Eger rift. We can find an extremely wide zone of sub-parallel faults (Měcholupy Fault Zone – Fig. 5) in this place. The narrow uplifted and dropped blocks of upper Cretaceous marlstones and lower Miocene limestones are separated by those faults. One of these faults are outcropped on the locality, the limestones are dragged along the fault (dip 48°).
In the nearby limestone mine, there can be found a slickensides planes with striations. General conditions of the locality are corresponding to a normal-fault activity; however the striations have been formed during the reactivation of the fault in a strike-slip regime.

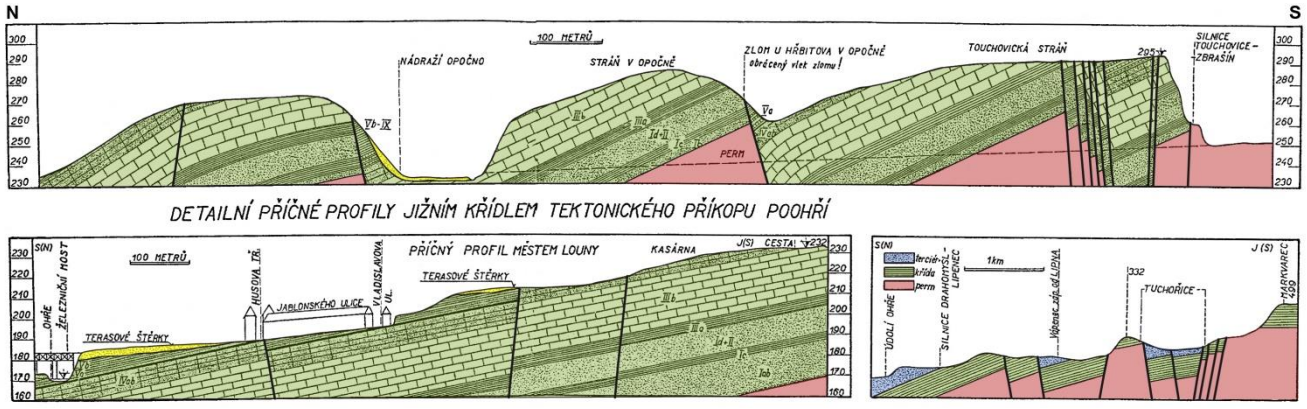

Fig. 5: A cross-section of the broad zone of the southern marginal fault of the Ohře Rift: the Litoměřice/ohře Fault between Louny and Tuchořice. After Váně (1964).

2a) Poláky - Hořenická (Erdbrandová) rokle: fluvial sediments embedded into the fault zone, paleostress analysis of the slickenside planes

(Coubal, M.)

The clays of Most Formation (lower Miocene), which are parts of the southern through of the Eger rift are disrupted by a series of small faults, are outcropped in the gully. The disruption is linked to a nearby Střezov Fault, which is crossed by Hořenice Fault Zone (NNW orientation) in this area. The disruption itself has been formed during the several tectonic phases. In the upper part of the gully, we can see a fluvial sediments (Pliocene or younger) embedded in the fault structures in underlying claystones. After the deposition of the fluvial sediments, Ohře incised to an underlying coal seam, uncovered it and a spontaneous ignition happened there. The claystones were transformed to porcellanites and the age of this metamorphosis was set by Tyráček et al. (1987) to middle or upper Pleistocene. It means, that the tectonic disruption of claystones is younger than the fluvial sediments but in the same time older than the metamorphosis. So it is a rare case of the preservation of slickensides of Pliocene/Pleistocene age.

Fig. 6: A slickenside cutting the claystones subjected to caustic alteration by an underground fire

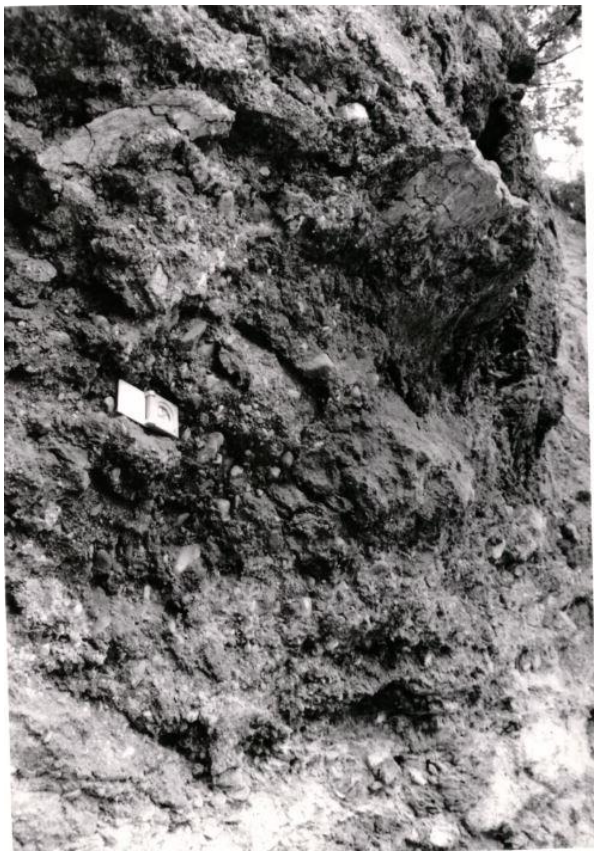

Fig. 7: Slickenside with tectonically embedded pebbles of gravels of a Pliocene or younger terrace of the Ohře River

Fig. 8: Historical photo of slickensides in the porcelanites of Most formation

2b) Poláky: landslide

(Hartvich F.)

On the southern coast of the Nechranice Lake a large active landslide was identified already in 1963, when the dam was still under construction. The area is formed by basaltic volcanic rocks, overlaid with Tertiary clays of Most formation (Fig. 9 and 10, 15, 19).
Due to the unstable conditions, the planned railway was moved further up the slope and the building was banned in the area. However, the building ban was lifted in 1985 and then the recreational colony (Fig. 9) spread on the temporarily inactive landslide (Dostalík and Malík 2015).
In December 2014, two shallow landslide developed in the recreational colony (Dostalík and Malík 2015). Firstly, small fissures developed, and started to spread and widen, finally forming a 2,5 m high headscarp, destroying several recreational houses(Fig. 11 and 12).
Currently, the landslide is stabilized, also due to five consequent years with low precipitation (2014-2019), however reactivation in the future is likely as practically no attempts of mitigation were performed. The report of Czech geological survey (Dostalík and Malík 2015) recommends renewal of the building ban, draining of the area of the landslide and decrease infiltration of water into landslide body.

Fig. 9:Poláky: The landslide documented in 1963 shown on 1955 topographic map (left) and 2011 topographic map (right). A and B are 2014 reactivations. While there are no buildings in 1960ies, during 1980 a recreational colony spread into the landslide area.

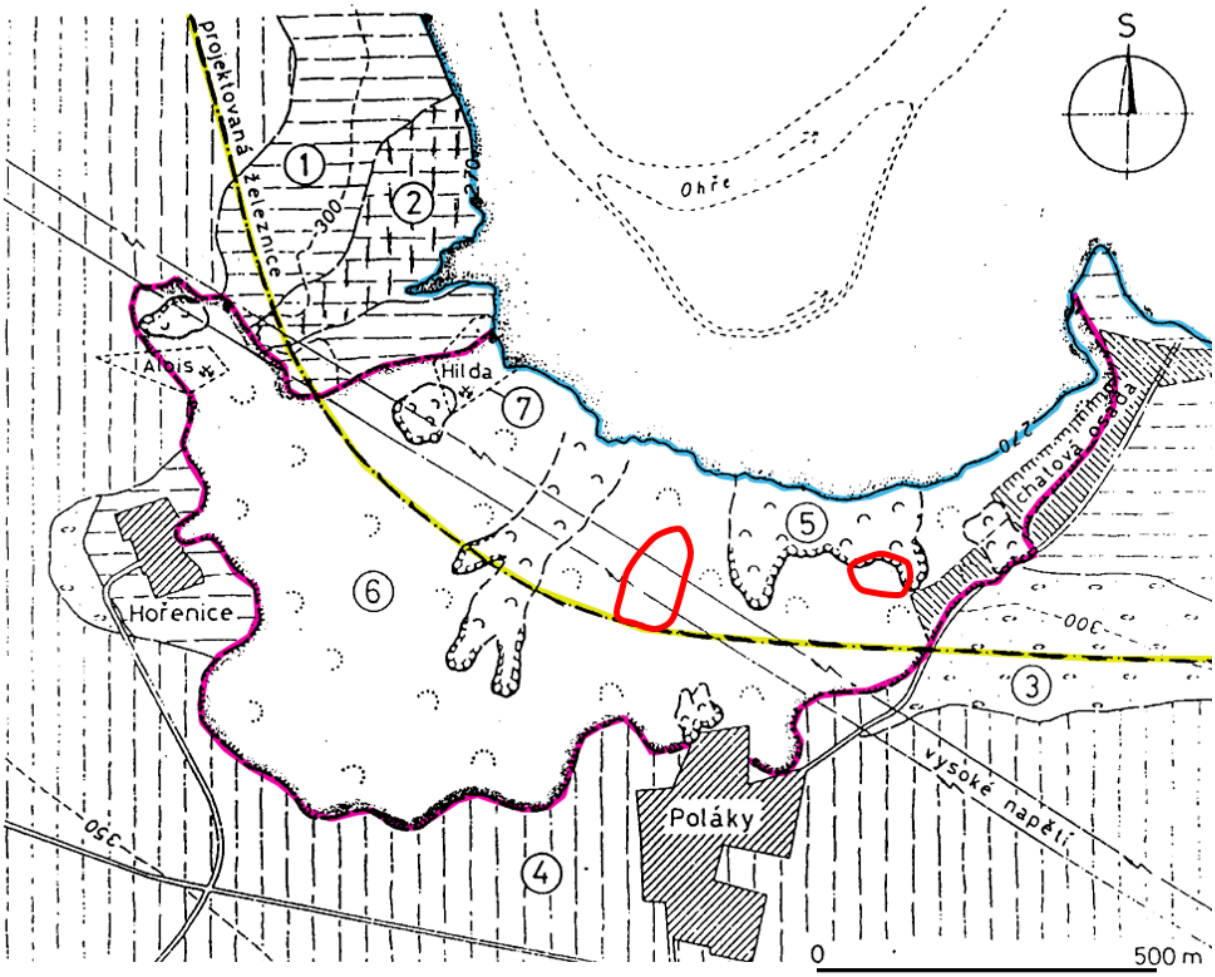

Fig. 10: Poláky: The original 1963 documentation of the Poláky landslide (after Rybář 1991) with 2014 reactivations (red line).

Fig. 11: Poláky: The The scarp and damaged house on the Poláky landslide (2014)

Fig. 12: Poláky: The scarp and damaged house on the Poláky landslide (2014)

3a) Nechranice dam: outcrop of the central rift fault (Střezov fault)
(Coubal, M.)

The Střezov fault is going along southern side of the central horst, its length is about 30 km from the volcanic complex of Doupovské hory Mts. towards NW. According to Malkovský (1979), the value of vertical drop of the SW block has been about 350m since upper Cretaceous.
On this locality, Střezovský fault (normal fault) is separating the pyroclastics of Střezov formation (Oligocene) and the siltstones and claystones (with beds of carbonates and coal sediments) of Most formation (lower Miocene). The slickenside plane of the fault was formed in thin layer of a clayish material; we can see also striations of a dextral oblique slip.

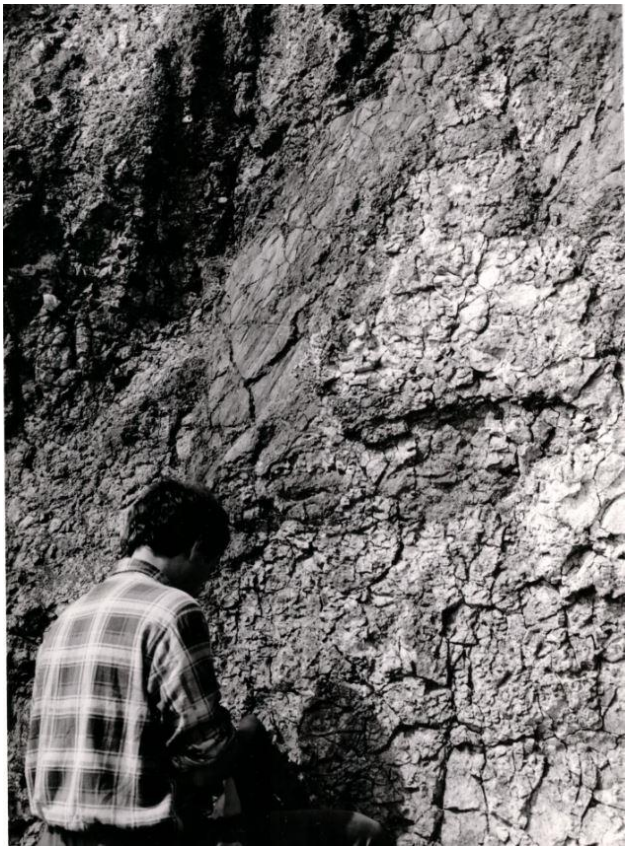

Fig. 13: Historical photo (1991) of slickensides in a limonite infill of the Střezovský fault

3b) Nechranice dam

(Hartvich. F.)

<u>Slumps and rockfalls</u>

The Nechranice dam (Fig 14) was built in 1960ies with several purposes, namely as a source of water for the nearby coal-heated power plant Tušimice, to control flood discharges and for recreation. The dam itself is 3280 m long, one of the longest earth-fill dams in Europe. Volume of the lake is 288 mil. m^3, area 13,4 km^2 and maximum depth 47,5 m.
Geologically, it is situated on slightly deformed clayey and marly sediments of the Most basin, formed in the Tertiary, locally overlaid with loess deposits. Thus the sedimentary bedrock is not very stable, and several types of slope deformations developed in and around the lake.
Practically since the construction started, the slopes around the dam were affected by various slope processes. The northern shore near the dam is affected by small slumps, related to strong abrasion of the coast by the erosive effects of waves. The slow sliding can be observed throughout the existence of the lake, with the coastline retreating significantly (1-10s of meters).

The slumps affect the most approximately 1,5 km long segment of northern shore (Fig. 15,16,17,18) along the water level. The scarps, 2- 12 m high, are visible above water level, and the accumulation can be found underwater.
Aside from slumps, rockfalls occur locally, as the tectonically disrupted claystones, silts and marls as well as loess loose stability particularly due to changes in water content and under freeze – thaw conditions.

Fig. 14: Aerial view of the southern part of the Nechranice dam (photo by Povodí Ohře)

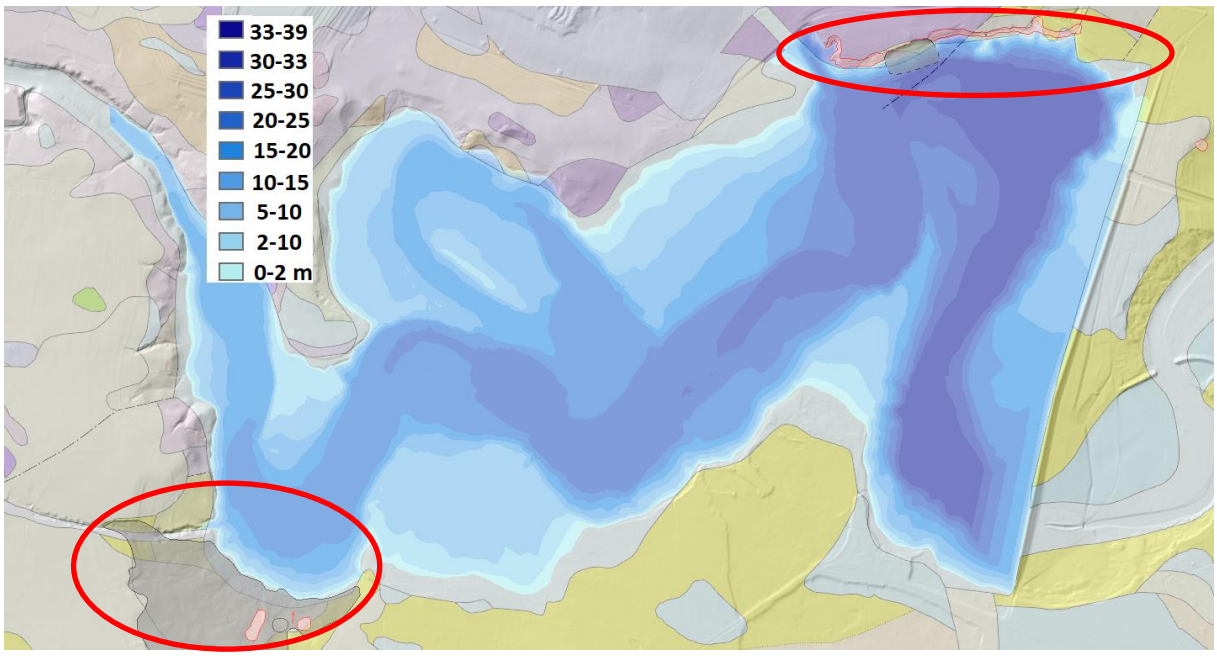

Fig. 15: Bathymetric map of the Nechranice lake. Red line indicates the areas with active landslides, northern shores (top right) and Poláky (bottom left). The colour scale shows the depth of the Nechranice lake.

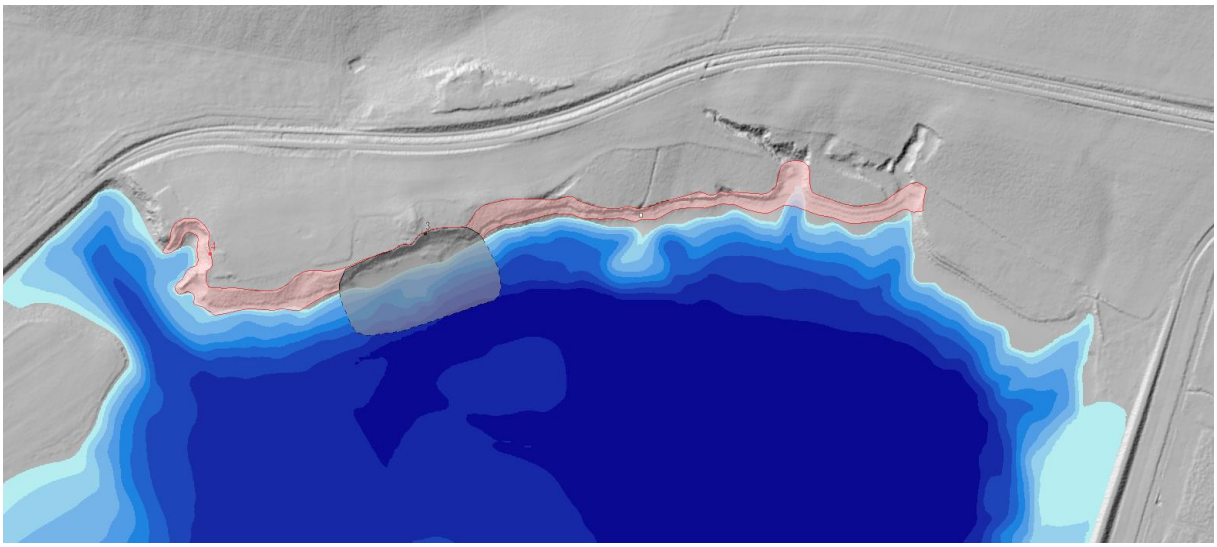

Fig. 16: Northern coast of the Nechranice lake affected by slumps, landslides and rockfalls in the length of about 1500 m (register of slope instabilities, Czech geological survey). Notice the underwater accumulations of the slumps shown by the isobaths.

Fig. 17: Nechranice dam: Back-tilted blocks of old slumps with conserved vegetation.

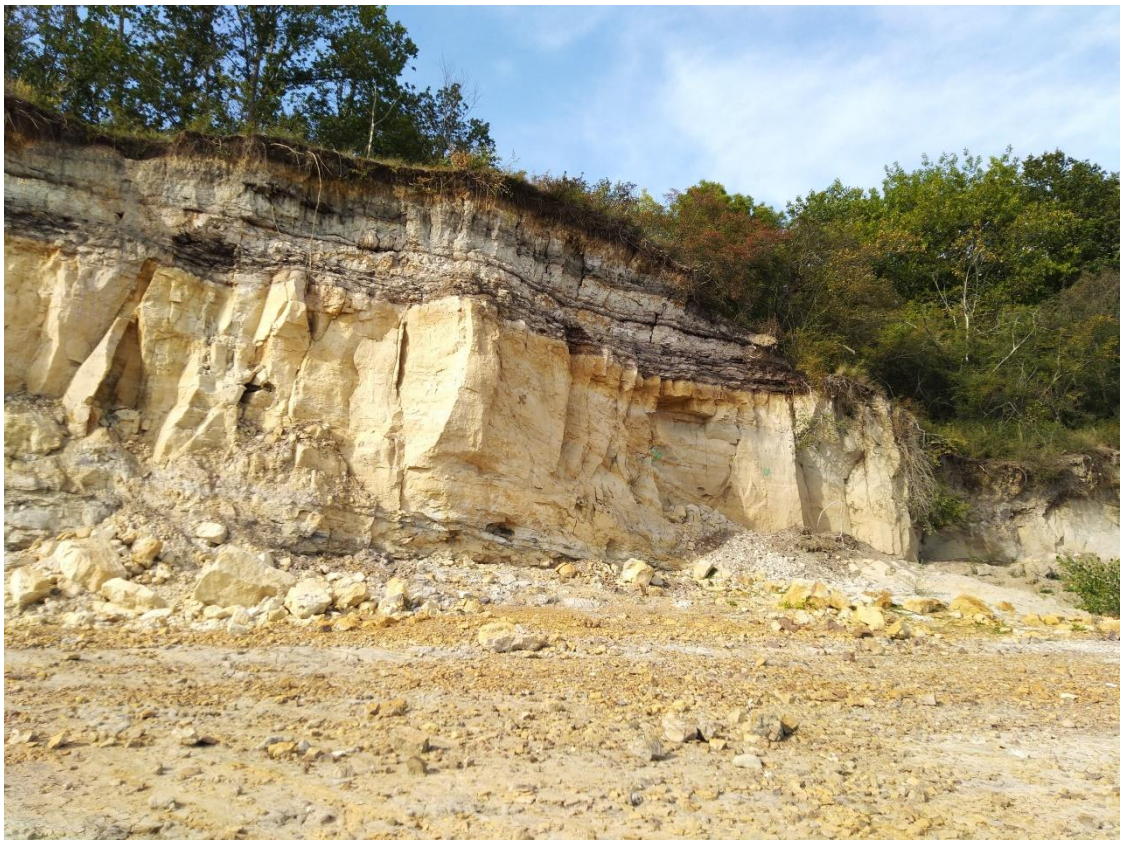

Fig. 18: Nechranice dam: Accumulations of small active rockfalls in clayey and silty sediments

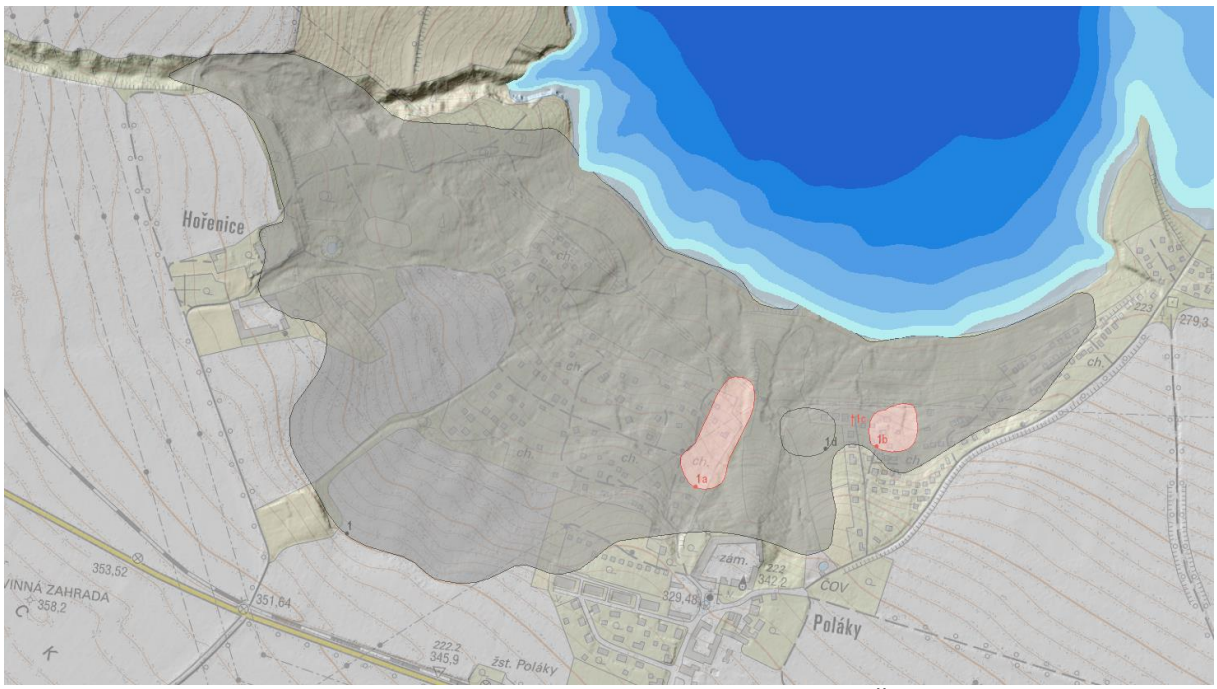

Fig. 19: Poláky: The landslide documented in the register of slope instabilities (ČGS) with 2014 reactivations. Hořenice gully limits the landslide from left side.

UAV remote sensing demonstration

Near-remote sensing using UAV

(Field method overview)

- UAV (unmanned aerial vehicle, commonly known as “drone”) is any aircraft without pilot present inside. It can be a helicopter, multicopter, plane, or glider
- UAV is component of UAS (unmanned aerial system) comprising UAV, ground-based controller and system of communication
- Usage for scientific (and commercial) purposes is regulated by Civil Aviation Authorities. Regulations depend on type, size and purpose
- Operator has to pass a theoretical and practical exam and has to have permission to fly and to perform fly works in a way to comply with the law (many restrictions and limitations)
- UAV flies over studied site, taking photos from various places and angles. The photos should overlap at least by 60% both along and across the flight path
- Changing of the camera tilt helps the processing.
- GPS position and tilt, roll and pitch of the vehicle is recorded in the EXIF table
- Flight and image collection can be programmed, but this is not allowed in many states
-

Structure-from-motion (SfM)

(Data processing method overview)

- SfM is an imaging method of using photographs to reconstruct 3D objects
- Principle is known since 1950s, but only recent evolution of computer processing power allowed its massive use
- Its accuracy can be compared to LiDAR with an advantage of evading the shade-effect. Depends on distance, pixel size, lens, aperture, and capture velocity.
- In geosciences, SfM is often used to create detailed DEMs or object models. For the collection of images, UAVs are often used. However, practically any camera, including mobile phones, can be used.
- Current software solutions (e.g. Agisoft PhotoScan/Metashape; Pix4D; Autodesk 123D; osm-Bundler; 123D Catch) allow fast semi-automatic processing to acquire 3D point clouds, meshes; adding textures and exporting DEMs, 3D models or orthophotos
- Recognizable control points (CP) should be established in the studied area and their position thoroughly measured (total station, GNSS)

- Example of data collection:

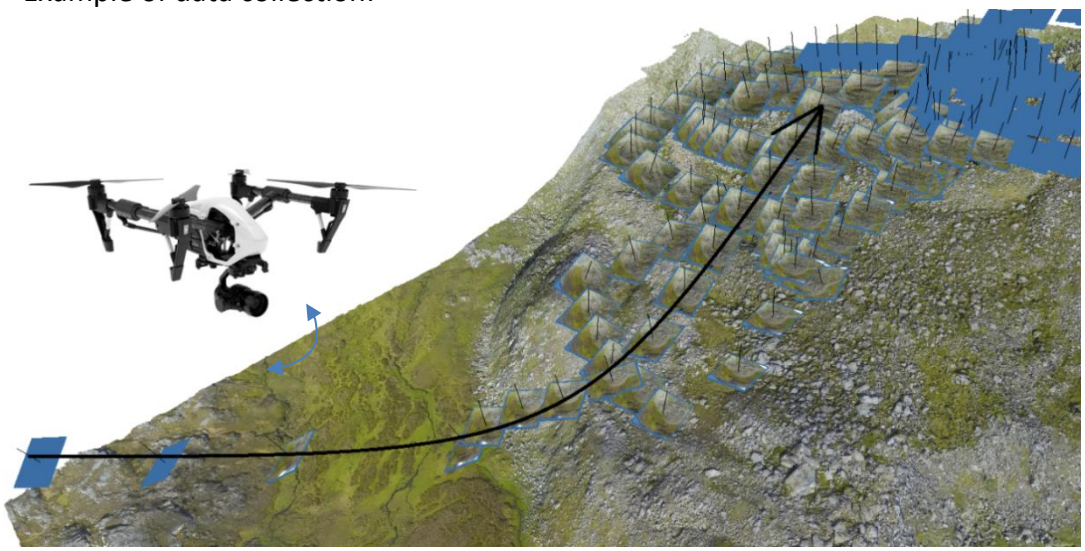

- Data processing workflow:

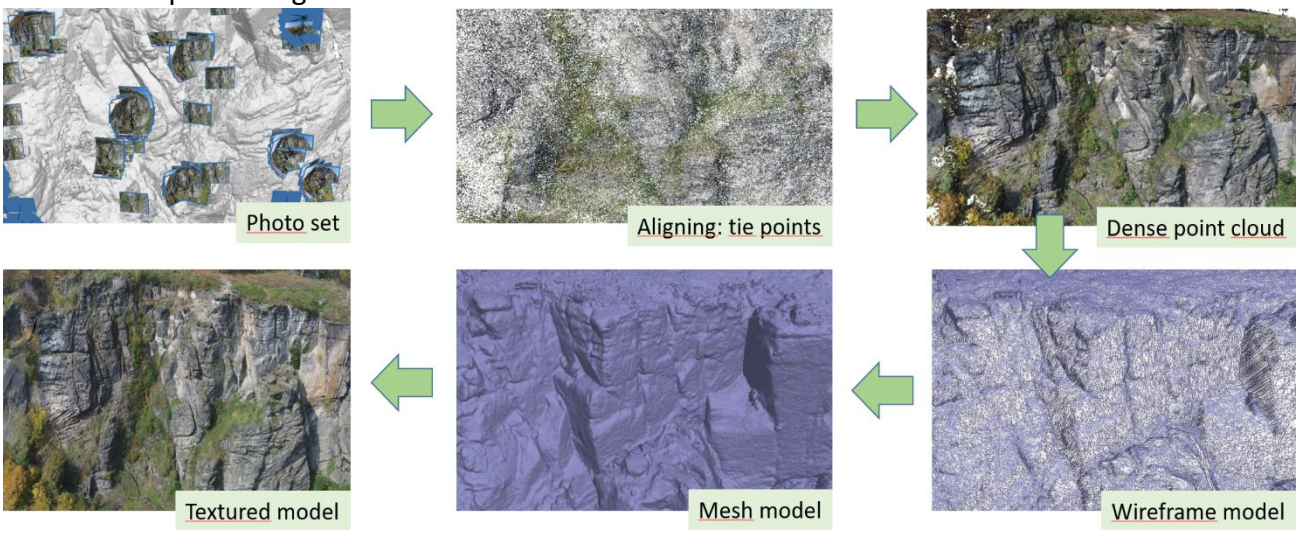

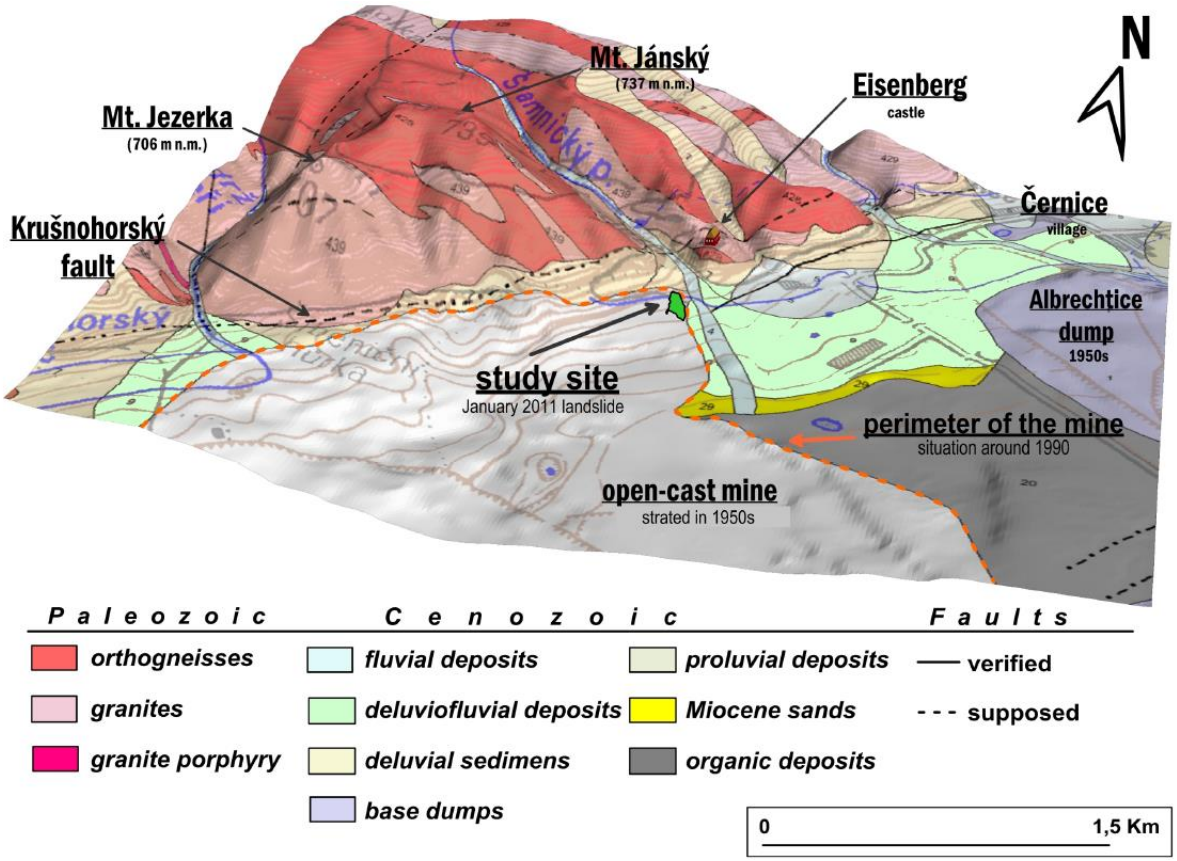

Fig. 20: Landslides Krušné hory: 3D geologic overview of the area of interest

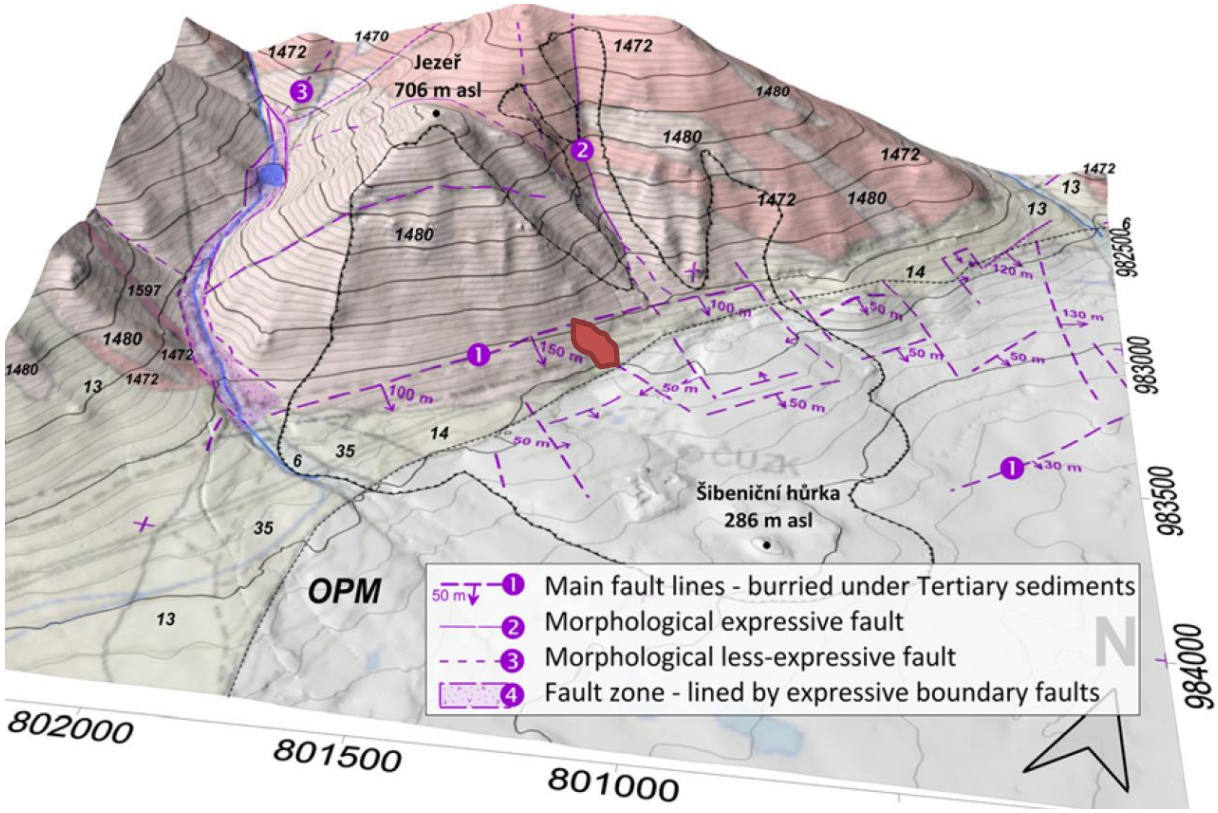

Fig. 21: Landslides Krušné hory: Tectonic setting and general overview of the landslide area at the foot of the Krušné Hory Mts (after Burda et al. 2018)

4) Vysoká Pec: Landslides along the foot of the Krušné Hory Mts.

(Hartvich F., Burda, J.)

The Krušné hory Mts. and the Most Basin present the main geological and geomorphological units in the study area. As a part of the Saxothuringian zone, the Krušné hory Mts. consist of crystalline complexes consolidated during the Cadomian orogeny and the mantle of Lower Paleozoic rocks weakly metamorphosed during Variscan metamorphism.
In general, the crystalline basement is covered by various heterogeneous sediments of the lower Miocene clays, sands, and sandstones as well as denudational relict material of the Upper Cretaceous and weathered volcanic rocks—phonolite, basalt, and tuff. These Paleogene sediments pass into Miocene coal sedimentation indistinctly. The boundary between the coal seam and the Miocene clay complex is sharp. The average fill of this overlying complex is approximately 175 m, with a maximum thickness of 231 m.
The Quaternary sediments predominately comprise coarse-grained gravels, sandy gravels, and clays with crystalline fragments. The thickness of sediments varies from 0.1 to 40 m (with an average of approximately 10 m) along the mountain foothills, and the rising thickness is associated with the alluvial fans or old fossil landslides. Maximum thickness of Quaternary sediment deposits (70 m) was found directly in the study site—around the Hůrka elevation under Mt. Jezeř (Fig. 20, 21).
The uplift of the Krušné hory Mts. in the Miocene–Pleistocene along the Krušnohorský Fault is expressed by the tilting of basin sediments near the edge of the mountains. Also, as a result of uplift, the foothills are characterized by numerous slope failures from the Miocene, Pleistocene, and late Holocene.
The landslides in the study area are situated in the foothills below the Mt. Jezeř (706 m) and Mt. Jánský vrch (736 m). Both south-east-facing mountains are characterized by having slopes with a gradient of more than 30°. On the Mt. Jezeř, the gradient can reach more than 40°, with the steepest parts situated on numerous rock outcrops. From east and west, the study site is delimited by the tectonically predisposed valleys of Šramnický brook and Vesnický brook (Fig. 20, 21)

The geomorphological setting is influenced by structural geological conditions, fault tectonics, periglacial and anthropogenic processes. In addition, it is also influenced by the headward erosion of the Šramnický Brook, which has incised a valley to a depth of 100 m. The relief is anthropogenic where the open-cast mine abuts the mountains. In this area 15m high overburden benches pass seamlessly into the steep structural slope of the mountains. The inclination of this anthropogenic slope is ca. 10–15° under the edge of open-cast mine, but in the mountains behind the margin of the basin the original crystalline slope is 30–40°. The main morphological processes that have modelled the anthropogenic slope during last two decades are those of stream erosion and mass movements.
In January 2011, a sudden inflow of warmer (7-16th January) resulted in rapid melting of abundant snow cover on the slopes of Krušné Hory Mts. This snowmelt became a primary trigger of the reactivation of an old landslide (Fig. 22, 23, 24), which historically caused the abandoning and deterioration of village of Eisenberg, situated on the margin of the Most basin at the foot of the tectonic slope of Krušné Hory Mountains.
This vast slope deformation was caused by mining for brown coal in the Most basin since the beginning of the 20th century. The mining lead first to depressions in the overlying sedimentary layers, and finally resulted into catastrophic collapse in 1952-54 landslide.

Afterwards, the mining continued in the form of open-pit exploitation, which deteriorated the stability of the slopes even further.
The Eisenberg landslide reactivation was the most significant event in the area of Most Basin since 2005 (Burda et al. 2012), when side slope of near open-pit mine collapsed as result of long-term rainfall culmination. While the studied landslide developed outside the open-pit mining area, it is part of a large, complex landsliding area, which is one of the largest runout landslides in the Czech Republic (Burda et al. 2018).

Current activity of the landslides is observed by VÚHU. Practically every year there are minor reactivation of some parts of the landslide-affected slopes, usually triggered by a collapse of weathered, tectonically weakened crystalline outcrops above the sedimentary basin margins (Fig. 25).

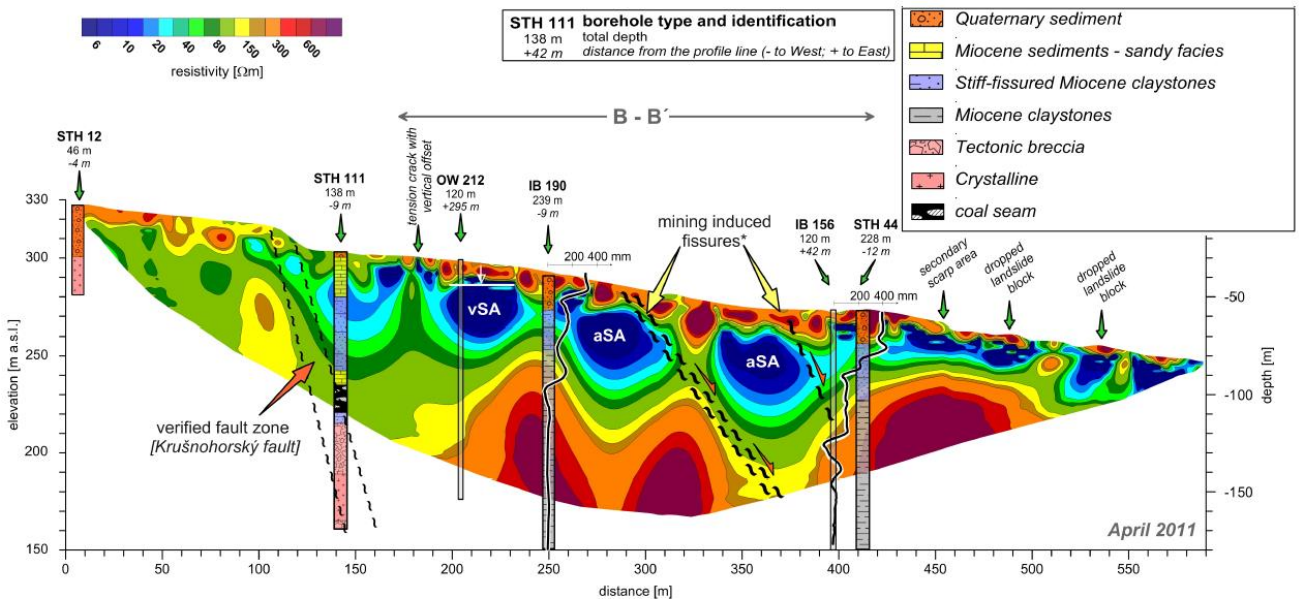

Fig. 22: Landslides Krušné hory: ERT profile along the landslide activated in 2010-11 (after Burda et al. 2012)

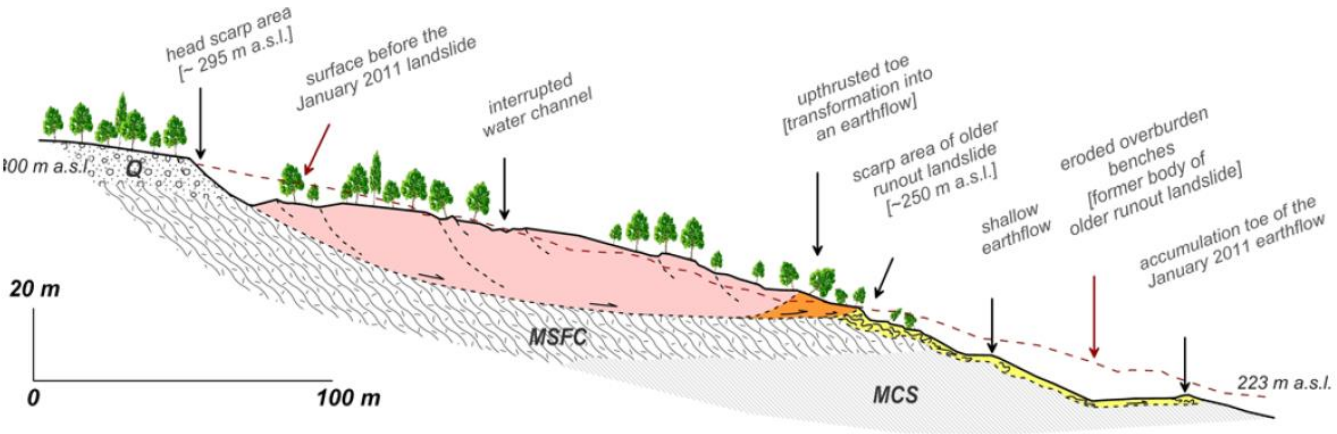

Fig. 23: Landslides Krušné hory: A schematic cross-section of the landslide activated in 2011 (after Burda et al. 2012)

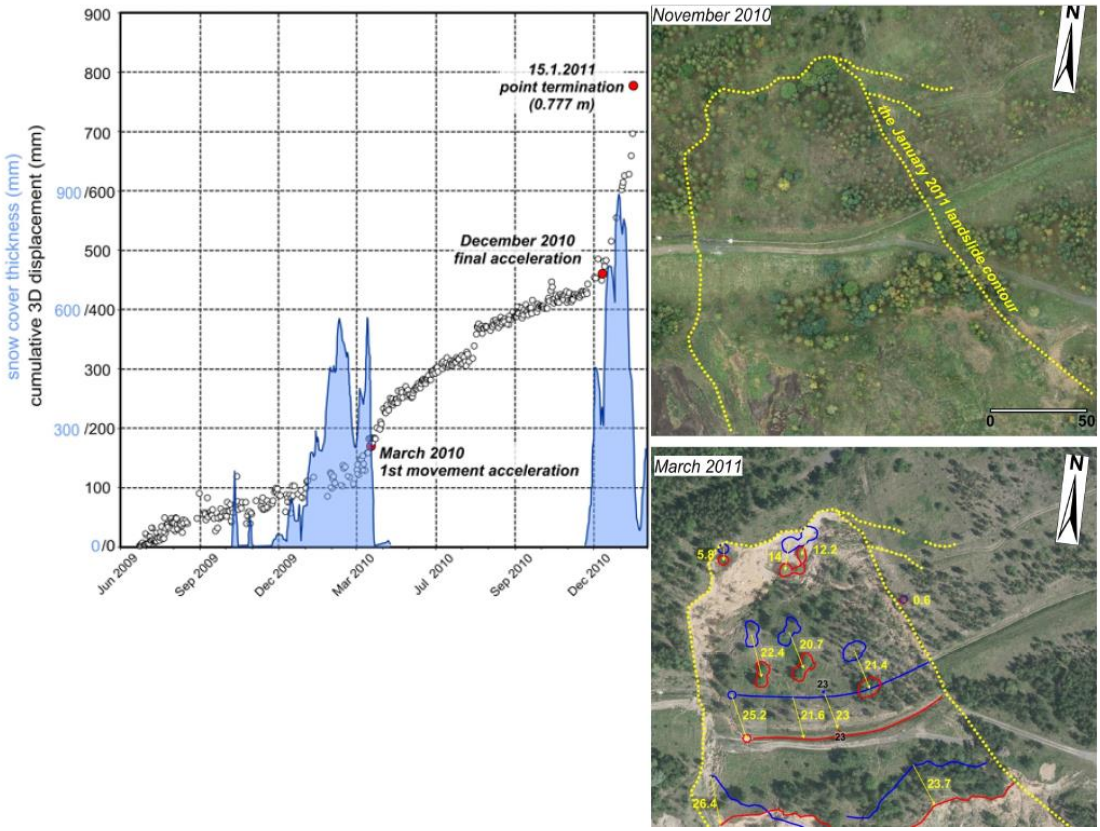

Fig. 24: Landslides Krušné hory:
Left: record of displacement of the landslide reactivation before collapse on 15.1.2011
Right: aerial photo of the reactivated landslide before and after (after Burda et al. 2012)

Fig. 25: Landslides Krušné hory: Fresh reactivation of landslides under the Krušné hory slopes (as of September 2019)

Friday 27th September

1) Introduction to Cheb Basin

The Cheb Basin (CB) is an asymmetric intracontinental basin that has evolved from the late Eocene until the early Pleistocene, and is filled with 300 m-thick deposits (Špičáková et al., 2000). Its origin has been controlled by several differently striking faults under a changing stress field, which has resulted in the formation of several sub-basins and its blocky fabric (Malkovský, 1987; Špičáková et al., 2000). The distribution of Plio-Pleistocene clastics shows the depocenter related to the Mariánské Lázně Fault (MLF), which testifies its late Cenozoic activity (Peterek et al., 2011). The MLF, which originated already in the late-Variscan as a normal fault with a dextral component and which alternated several different kinematics (Pitra, 1999), is also expressed in the present-day topography by the pronounced escarpment to the east, which is about 200 m high in the area of CB and which controls the eastern mountain front of the Krušné hory Mts. (Fig. 26).

The stratigraphy in the CB can be simplified and divided into three intervals (Malkovský, 1995; Špičáková et al., 2000) (Fig. 1). The Pre-Cypris strata (Late Oligocene to Early Miocene, ca. 26-21 Ma) group together the Lower Clay and Sand Formation, including volcanics and volcanoclastics and the coal seam formation. The Cypris Formation (Early to Middle Miocene, ca. 21-17 Ma) is characterized by widespread lacustrine conditions with dominant clay lithologies. The Vildštejn Formation (Late Pliocene-Pleistocene, ca. 4.5-1.4 Ma; Bucha et al., 1990; Špičáková et al., 2000; Teodoridis et al., 2017) was deposited discordantly after a hiatus of 12 Ma duration. Its fluvio-lacustrine sediments consist of kaolinic clays, sands and gravels (Fig. 27, 28). During this period the NW-trending faults controlled the shape of the basin depocenters, especially the MLF as a master fault. Špičáková et al. (2000) proposed that the MLF acted as a sinistral strike-slip fault under transtension, although they mentioned also some contradictions (see also Rojík et al., 2014). The asymmetric subsidence was accompanied or followed by the uplift of the footwall with the Krušné hory Mts., which resulted in separate evolution of the formerly united Cheb and Sokolov basins (Špičáková et al., 2000; Pešek et al., 2014). The Vildštejn Formation together with the Pleistocene Ohře river terraces was also faulted by the MLF, as documented by Ambrož (1958).

The last volcanic episode during the Pleistocene in CB is represented by the scoria cones Komorní hůrka/Kammerbühl and Železná hůrka/Eisenbühl (Ulrych et al., 2003; Geissler et al., 2004) and by the newly discovered Mýtina Maar (Mrlina et al., 2007, 2009). These small volcanoes are located at the flanks of the Eger Rift (Geissler et al., 2004) (Fig. 27) and are characterized by a phreatomagmatic initial stage and an eruptive final stage of volcanic activity. Age determinations of the olivine-nephelinite lava (Seifert and Kämpf, 1994; Mrlina et al., 2009) indicate that the Quaternary volcanism occurred in the mid-Pleistocene 0.78–0.12 Ma (Šibrava and Havlíček, 1980; Wagner et al., 2002; Ulrych et al., 2003; Mrlina et al., 2007.

Active and passive seismic studies were carried out to reveal the character and depth of the crust-mantle boundary in the CB area (Hrubcová et al., 2005, 2013; Hrubcová and Geissler, 2009). The present model for the crust consists of a highly reflective top of the lower crust at depths of 27-28 km and an underlying laminated structure of the Moho. According to Geissler et al. (2005) the features of the lower crust may be interpreted as low-angle shear zones containing fluids and/or small magmatic intrusions (sills/dykes) or partial melting. The observed structure was interpreted as magmatic underplating (Hrubcová et al., 2017) based

on the absence of seismic reflections in the zones of increased seismic velocities, which could be related to the Quaternary volcanism in the area. In the CB, earthquake swarms are related mainly to the Nový Kostel focal zone, which dominates the seismicity of the whole West Bohemia/Vogtland area (Fig. 27). This is the location of all the $M_L \geq 3$ swarms during the last 30 years (one swarm in 1985 and 6 others between 1997 and 2018), wherein hypocentres were precisely determined with instrumental data. The focal zone trends NNW and crosscuts the MLF, suggesting no relation of the present earthquake swarms to the MLF (Fischer et al., 2014). Historical records show several earthquakes that could be associated to the southern continuation of the MLF within the Cheb-Domažlice Graben, with intensity I_0 from 4.5° to 6.5° MSK. The unknown focal mechanisms of these pre-instrumental earthquakes, however, prevent us from verifying their tectonic relation to the MLF.

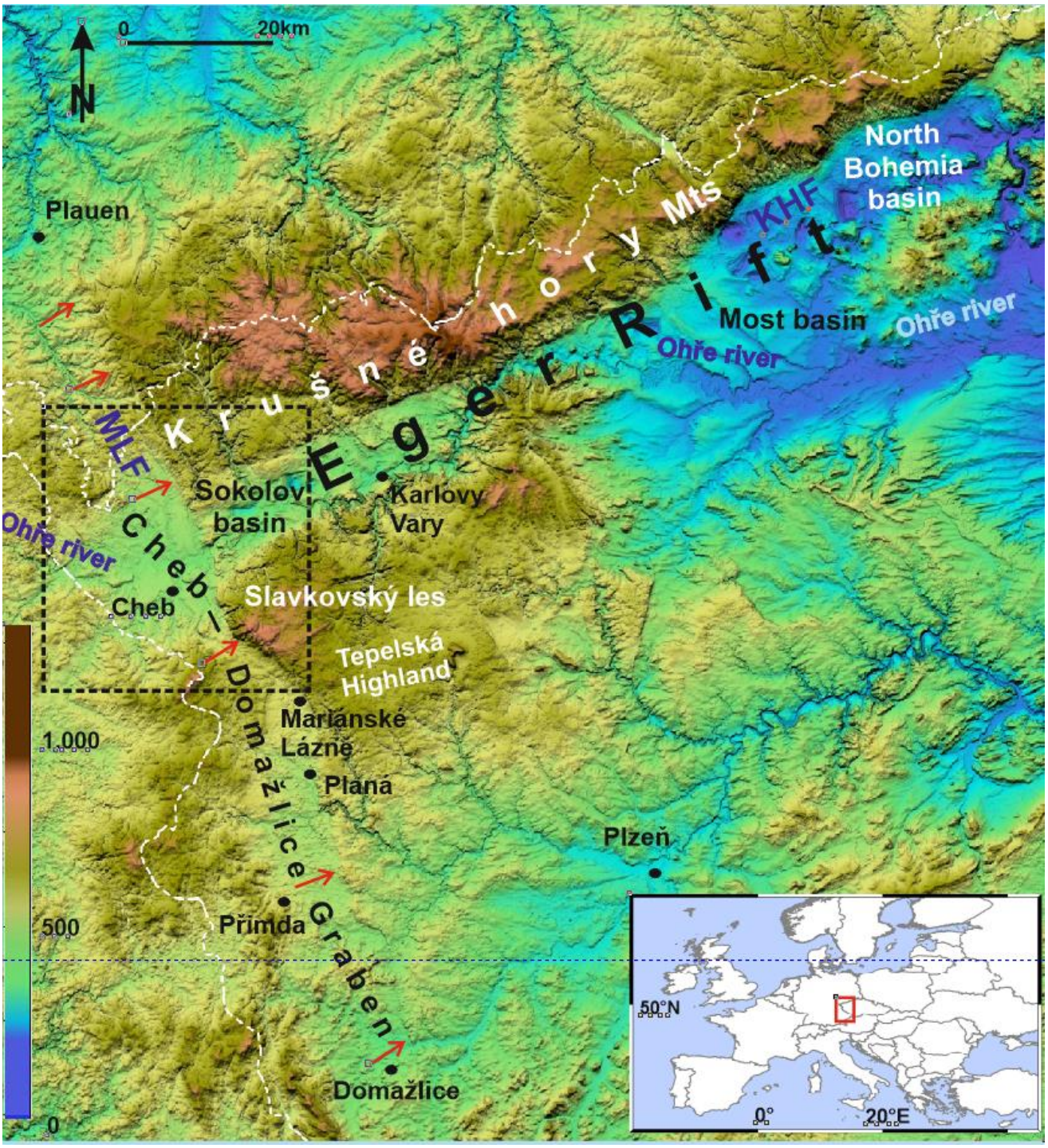

Fig. 26: DEM of the Eger Rift and Cheb Basin

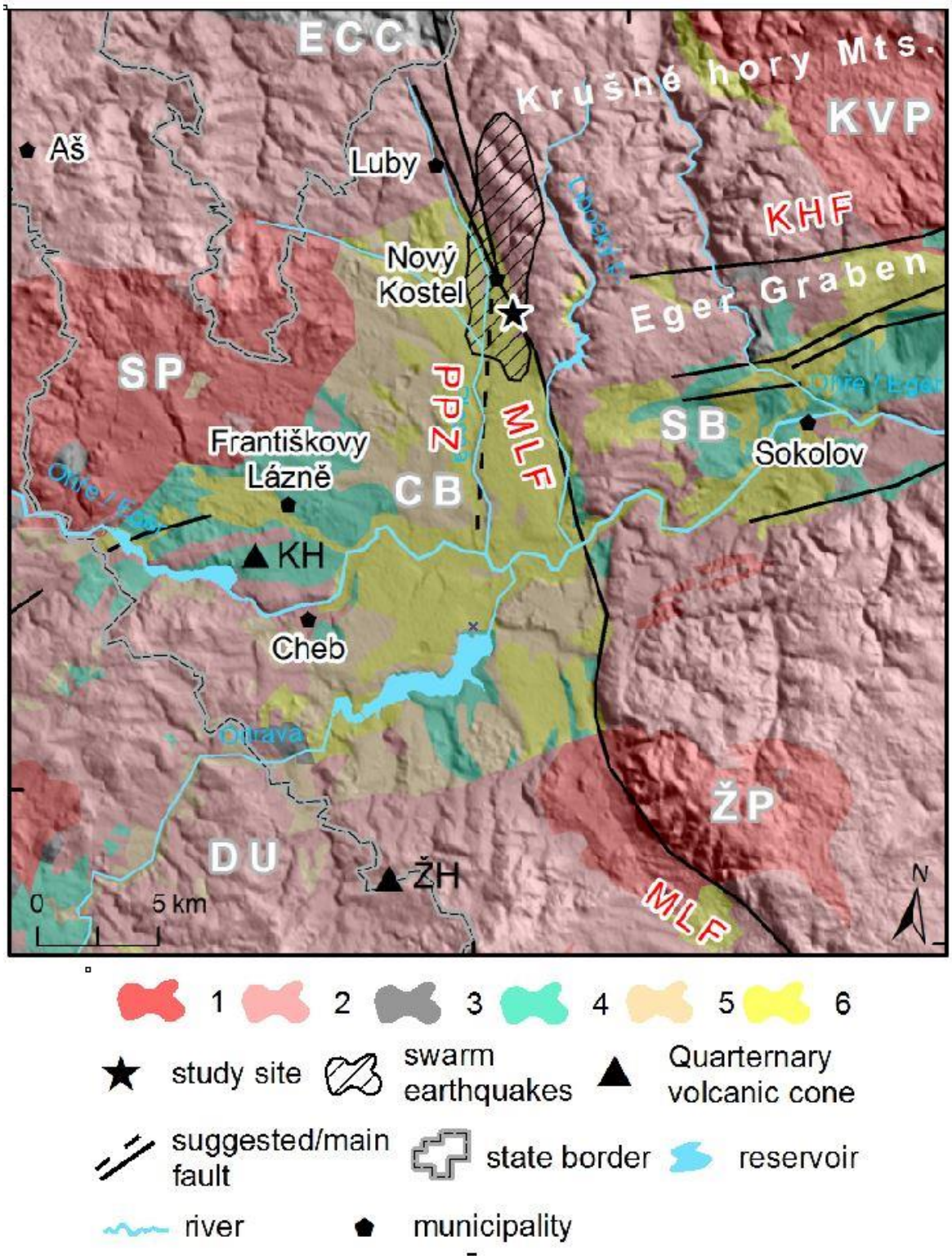

Fig. 27: Geological map of the Cheb Basin. 1 – Late Variscan granites and granitoids, 2 – Variscan metamorphic units, 3 – Volcanics (mainly Oliocene/Miocene), 4 – Miocene (Cypris Formation), 5 – Plio/Pleistocene (Vildštejn Formation), 6 – Quaternary; ECC – Erzgebirge Crystaline Complex, DU – Dyleň Unit (granitoids), SP -Smrčiny pluton, KVP – Karlovy Vary Pluton, CB – Cheb Basin, ŽP – Žandov Pluton, SB – Sokolov Basin, ŽH – Železná Hůrka volcano, KH – Komorní Hůrka volcano, PPZ – Počátky-Plesná Zone, MLF – Mariánské Lázně Fault

2) Soos – nature reserve with mofettes

Soos is a locality with very strange name – it is not Czech, neither German. Probably it came from a German word “Satz”, which could mean something like deposit, sediment or a marsh perhaps. The transcription “Soos” is just a form of this word in a local Egerland (Chebsko) dialect of German.
Soos is an example of a unique territory on a pan-European scale and includes a wide variety of biotopes and their transitional phases. On the nature reserve territory we can find peatbogs and fens with numerous issues of mineral water and emanations of gaseous carbon dioxide, extensive water surfaces and small streams. The central part of the reserve contains a notable diatomite deposit, saturated with mineral salts. Local plant communities represent a varied mosaic of the vegetation of high-moor bogs, transitional peat-bogs, fens, halomorphic soils and communities which are directly influenced by the CO_2 gas emanations. The diversity of animal species, especially of invertebrates, amphibians and birds, is also of exceptional natural value (Rajdlová, 2011).

The Soos lies in the central part of the Cheb Basin (Fig. 27, 28) and it is originally the shallow basin formed by fluvial erosional processes. In the beginning of Holocene period, this depression started to be filled by rainwater and particularly by the rising mineral waters. Because of the sufficient influx of water, the bogs and fens have been formed in the area. The different composition of the mineral waters in the various parts of the locality leads to high variability of formed sediments (Fig. 29). Also, the mineral waters were an ideal environment for growth of the algae and diatoms. Therefore, interesting layers of diatomite were formed in the central part of the area. The bogs are present mostly in the outer part of the nature reserve, based on the rainwater or on the waters of a calcium-magnesium-hydrogencarbonate type. Fens of the humolite type were predominantly formed in the central and southern parts of the nature reserve, in areas with waters of a sodium-hydrogencarbonate type and also where the waters with low content of dissolved solids mixed with acidulous waters of a sulphate-hydrogencarbonate-chloride-sodium type with high contents of dissolved solids. Sulphur-iron-rich fens have formed in some areas on the diatomites. Fens with pyrite content (mostly black or more rarely in the form of silver crystals several millimetres in diameter) where the sites favourable for the origin of limonite and palliardite as well as minerals formed by water evaporation such as sodium sulphate, sodium carbonate, calcium sulphate and sodium chloride. Ferrous sulphate and ferric sulphate can be also found at places where the diatomites are exposed to air oxidation. Especially in dry periods these minerals form extensive salt efflorescences in areas without vegetation (its growth is inhibited by extremely acidic soil and water environment due to the effects of sulphuric acid) (Rajdlová, 2011).
The interesting phenomenon, besides of the springs of mineral water, are the mofettes. These are the places of emanation of carbon dioxide, which has its origin in the crystalline basement of the Cheb Basin and it is representing the final phase of the volcanic activity in the area (see below). The carbon dioxide can be emanated into a small depressions filled by water – and create a bubbles on the surface; or by mud and form a feature similar to a mud volcano. However, carbon dioxide can be accumulated (due its bigger density that the air) in dry depressions, which can be a dangerous trap for insects, birds and other small animals (Rajdlová, 2011).

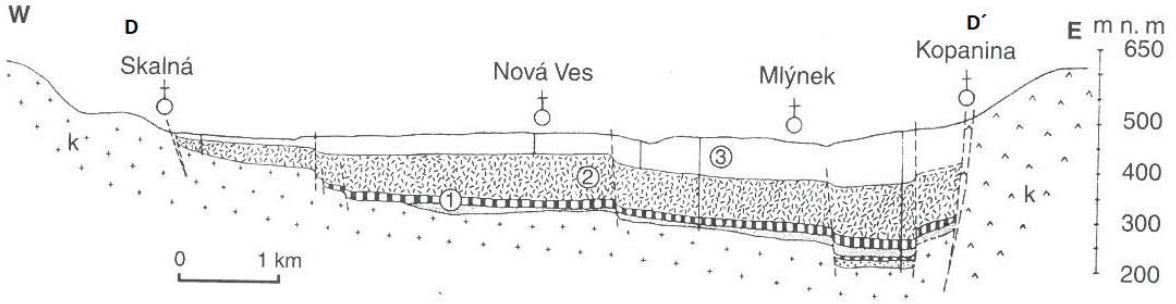

Fig. 28: A cross-section of a Cheb Basin (after Šantrůček, 1964 in Chlupáč et al., 2011). k – crystalline rocks, 1 - "Pre-Cypris" strata , 2 – "Cypris" formation (lower Miocene), 3 – Valdštejn formation (Pliocene)

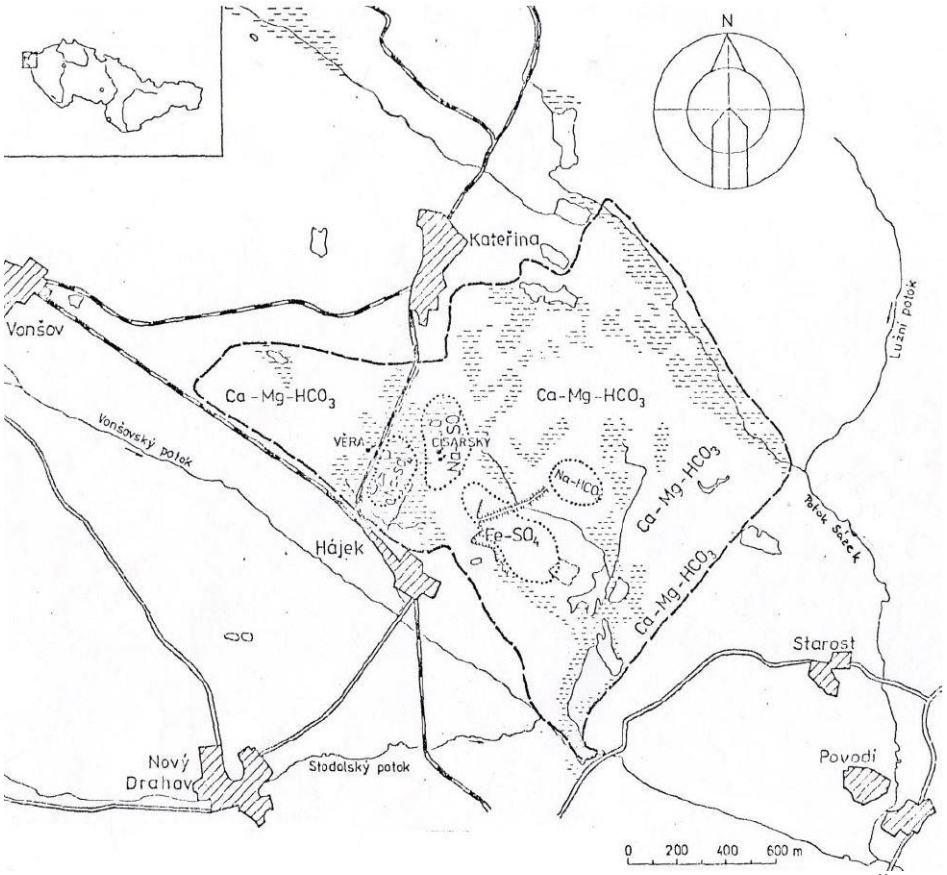

Fig. 29: Soos nature reserve with the areas of different composition of mineral waters (after Řeháková, 1988 in Rajdlová, 2011)

3a) Skalná: Geodynamic observatory and seismic station in Skalná

*(**Fischer T**., Mrlina J., Polák V.)*

In the seismoactive region of West Bohemia (e.g. Fischer et al., 2014) continuous detailed seismological observations were initiated after the earthquake swarm in 1985/86, which resulted in WEBNET seismic network established in 1994. The SKC seismic station was built in an underground gallery of a granite outcrop in the town Skalná at the western edge of Cheb Basin. Later, geodynamic observations have been introduced to the West Bohemia region in mid-90-ties: GPS and precise levelling for surface displacement control, repeated gravity measurements aimed at mass/stress redistribution monitoring, and groundwater level observations (Mrlina, 2000; Mrlina et al., 2003) and seismic station SKC has been converted into a complex geodynamic observatory. The aim was to monitor continuously the ongoing geodynamic processes and to improve our chance to detect potential precursory phenomena preceding earthquake swarms.

The multiparameter observatory is thus equipped with a seismograph, a couple of tiltmeters, a barometer and a strainmeter and continuous measurements of gravity to evaluate local changes of gravity field (Fig. 31). Significant signal was recorded during the Sumatra earthquake in Dec. 2004 by the LCR Graviton EG apparatus. The records document the fact that even distant regional and global events can lead to consequent redistribution of stress and mass that are detectable by sensitive gravimeters (Mrlina in Boušková et al., 2007).

3b) Skalná: Fault monitoring using TM-71 3D dilatometer

(Hartvich, F.)

An optical-mechanical 3D dilatometer TM-71 (Fig 30) was originally developed during the 1960s by Ing. Košťák (USMH). It was intended for monitoring three dimensional crack development within man-made constructions such as tunnels and bridges, however, it is now used to quantify fault displacements, slow moving landslides, and to assess the effect of the landslide mitigation measures.

The TM-71 device uses moiré patterns to quantify displacement, observed on two pairs (horizontal and vertical) of identical, overlying glass plates with etched spiral grid and one pair of rectangular grids. The circular grid produces a moiré pattern in the form of hyperbolical lines, while the rectangular grids produce a moiré pattern in the form of parallel angular lines. The moiré patterns recorded on the spiral grid measure the displacement, the rectangular grids measure the rotation.

The sensitivity of the device is governed by the density of the applied grids. The grids usually range from 8-100 lines per mm (Košťák 1969). With high density grids, the device is able to record relative displacements or deformations (Fig. 32) in three co-ordinates (*x*, *y*, *z*) with accuracy of better than ± 0.007 mm (Stemberk et al. 2010). It also records horizontal and vertical rotations (*gxy* and *gxz*) with accuracy of better than ± 0.00016 rad (Košťák et al. 2011).

The device is mounted across a discontinuity using two connecting arms, drilled into the rock walls on either side of the discontinuity, and cemented. The reading can be done manually on photopaper using a photoflash, or a digital camera, or the device may be automatized, using pair of cameras, backlights and special computer. This however requires source of electricity or a battery.

The first TM-71 device was installed in the cellars under town of Skalná in 1998. The monitoring was renewed in 2018, when a second device was added on another fault and both devices were automatized. The monitored faults are part of the tectonic system limiting the Cheb basin.

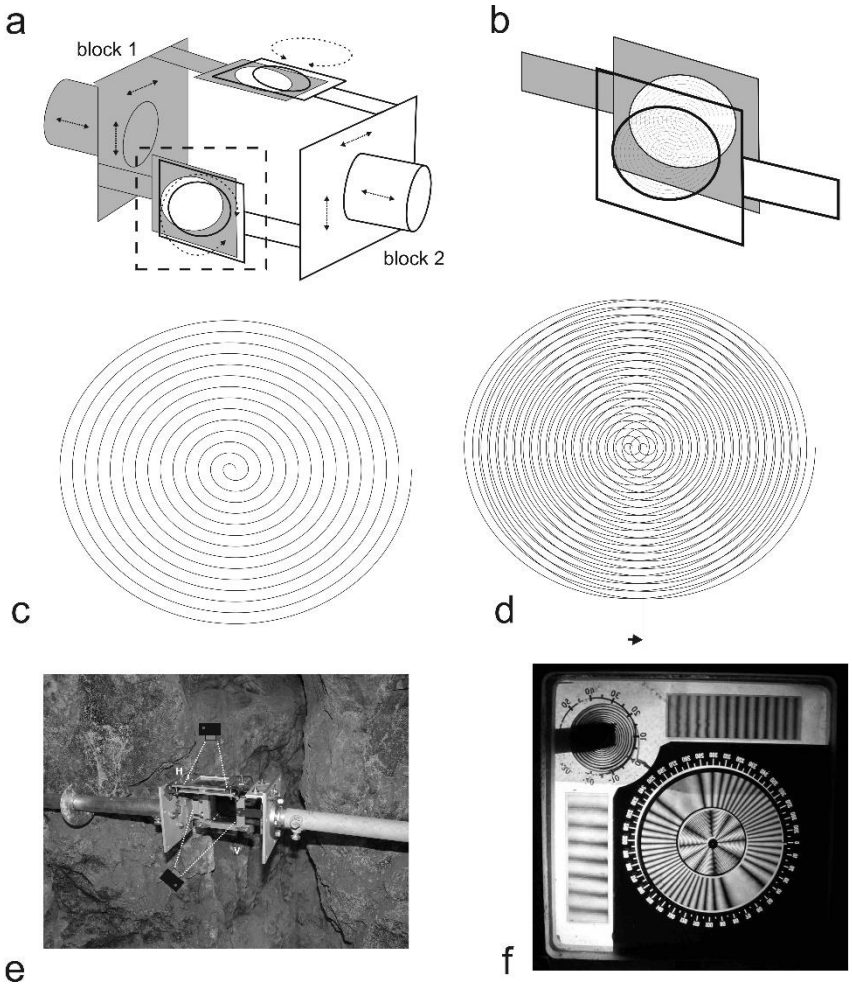

Fig. 30: An optical-mechanical 3D dilatometer TM-71

Fig. 31: Gravimeter Graviton EG during data transfer (left), and the recording unit of tiltmeters (right). The tiltmeters are covered by plastic sheets.

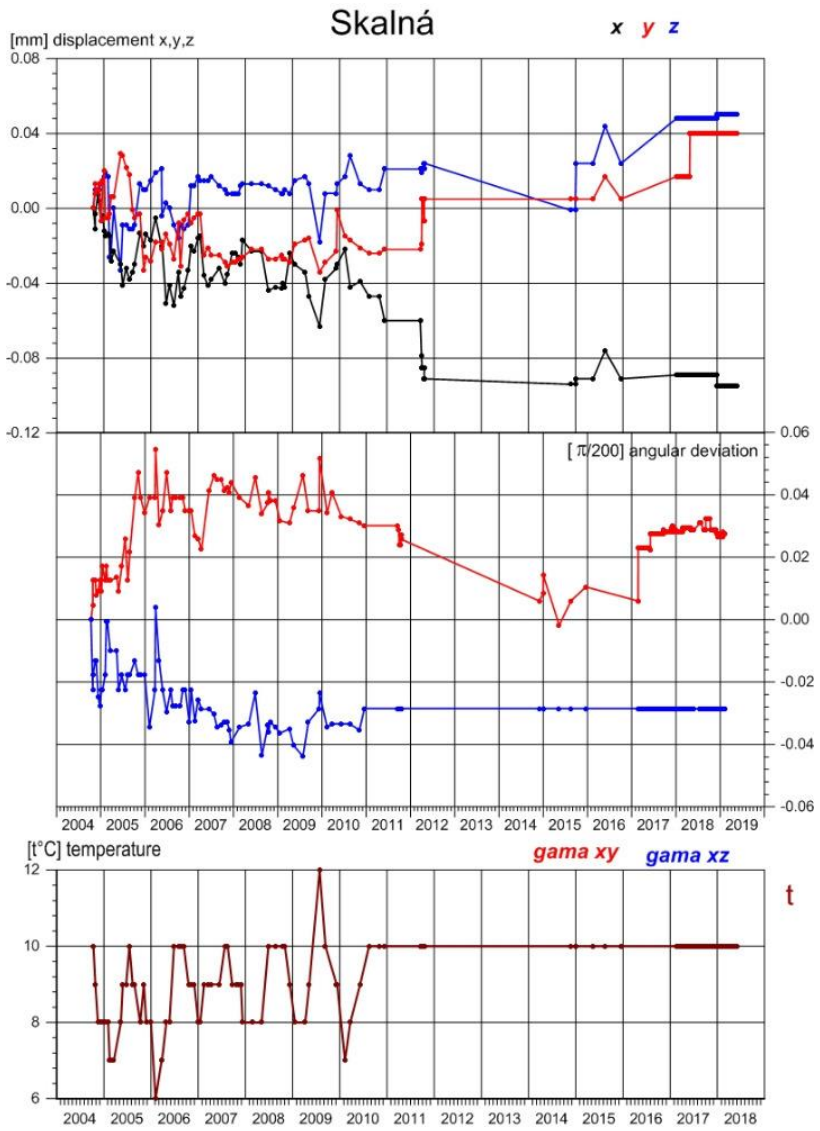

Fig. 32: The results of measurement with 3D dilatometer TM-71 (displacement x, y, z; angular deviation, temperature)

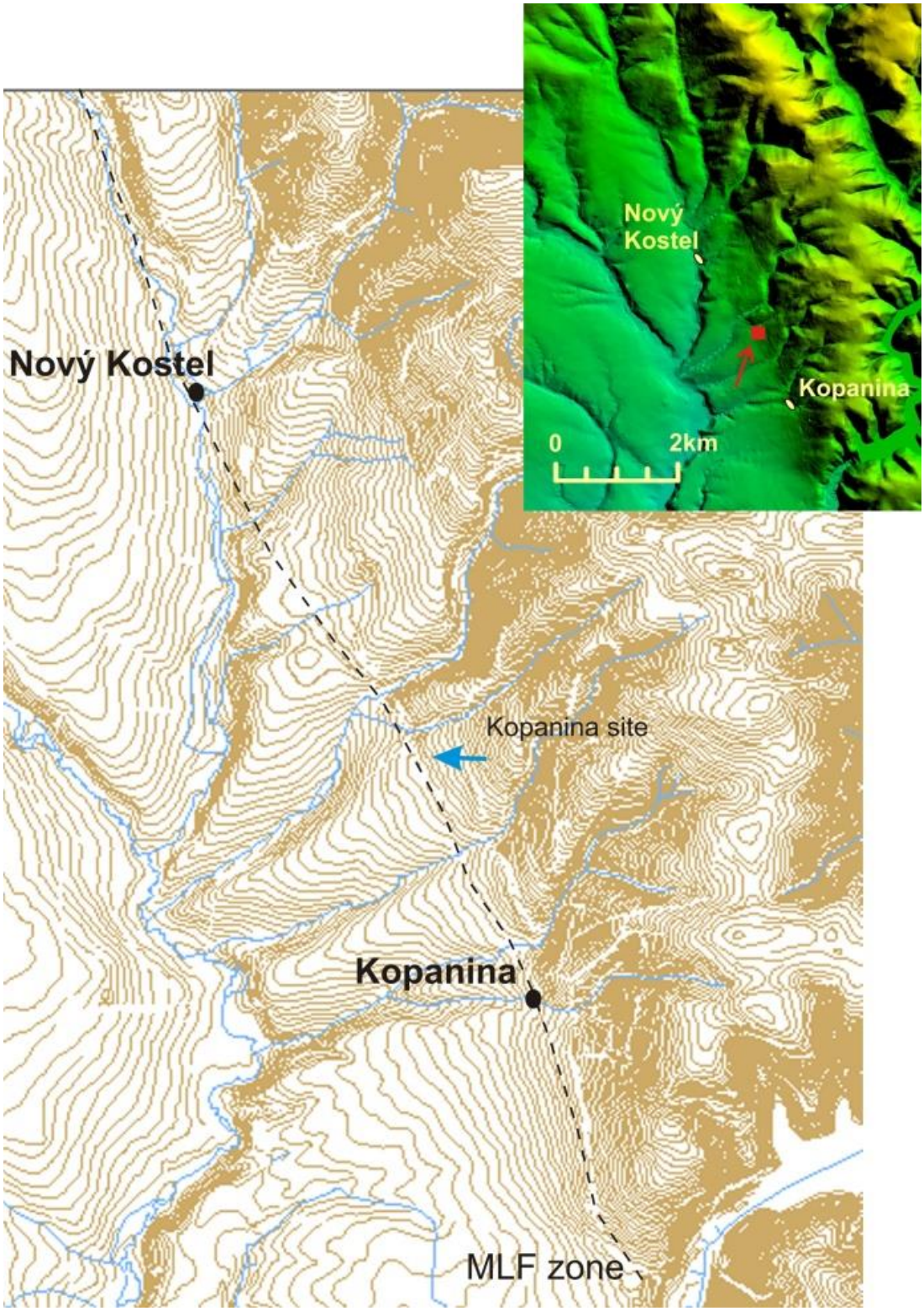

Fig. 33: Mariánské Lázně Fault zone indicated by foothill and linear arrangement of beginnings of deeper valleys with position of Kopanina trenching site

4a) Kopanina: Fault scarp morphology within the Mariánské Lázně fault zone, paleoseismic trenching site

(Štěpančíková, P.)

The site is situated at the mountain front line of the Krušné hory Mts. controlled by the northern termination of the Mariánské Lázně Fault (MLF) between Kopanina and Nový Kostel villages. The fault trace is suggested by a linear arrangement of points where series of sub-parallel valleys become deeply incised into an apparently uplifted blocks and by a gentle convex-shaped scarp, which is linear along a length of several hundred meters and was supposedly controlled by the MLF. (Fig. 33). Geophysical survey – ERT (electric resistivity tomography) and morphological analysis enabled to place a fault-crossing paleoseismic trench of 100 m length, and varying depth of 1.5 to 2.5 m at Kopanina site. Later, based on the findings, four additional fault-crossing trenches and two fault-parallel ones were excavated. They exposed a succession of sedimentary units of the Cheb basin, whose lithologies and stratigraphic interpretation are shown for Trench A in Fig. 34.

The simplified description of the sedimentary units downhill is as follows: in the upper part of the trench Tertiary clayey-sandy colluvial sediments (unit *b*) cover completely disintegrated, chemically weathered mica-schists basement *(a)*. Following inclined beds (units *e)* of probably Staré Sedlo Formation (upper Eocene to Oligocene) consist of basal conglomerates with ferric cement, heterogenous units of poorly sorted sandy gravels with clayey silty matrix, and reworked gravely sands with ferricretes. This formation is terminated by the fault F4 striking at 162° towards the following Plio-Pleistocene Vildstein Formation (units *f*), which is formed by diagonally stratified fine gravels and sands. These sediments are disturbed by minor sub-parallel 137°-142° striking normal faults F3 with offsets of ca 10 cm. Further downhill, up to 45° tilted heterogeneous layers of overlying fine gravels and sands are cut by the sub-vertical fault F2 with strike of 132°. This fault filled with white clay is accompanied by distinctive iron mineralization penetrating laterally. The capping layers *(g1)* were dated by OSL as ca 170-204 ka. The following layers of clayey sand are downwarped and deformed by the youngest 134° striking fault F1, which separates them from deformed stratified coarse sands to the southwest. We consider the structure as push-up due to seismic event. This youngest fault coincides with the slightly convex morphology of the fault scarp on the foot of the slope. The youngest Holocene sediments, units *h1* and *h2*, downwarped and cut by this fault F1 with max. displacement 0.39 m were dated by radiocarbon dating method as ca 0.9 to 5.3 ka BP. In the lowest part of the trench clayey sand to clay is overlain by loamy gravelly colluvium, partially folded and displaced by minor faults with minor offsets (up to 10 cm).

Based on the empirical relationships of rupture length (identified by using LiDAR images) and vertical displacements measured on the faults in the trench, versus magnitude, the size of the seismic events responsible for the revealed deformations was assessed to a minimum moment magnitude Mw=6.3 to 6.5. The events timing is shown in table 1. Two youngest events were dated to Holocene (1134 – 192 BC; and 792-1020 AD), and resulted in a push-up structure formation and displacement in tens of centimetres. The latter event appeared to be historical and the most probable candidate earthquake is the event of July 998 AD reported in the catalog of Kárník (1957) and the catalog for Central and Southeastern Europe (Shebalin et al., 1998) with macroseismic estimates of magnitude M=6.2 and estimated epicentre coordinates 50.4N, 13.4E (close to Chomutov), which is only about 70 km north-

east from our trench site Kopanina. It should be noted that the accuracy of epicentre coordinates estimated from historical macroseismic observations is very poor, especially for the period of interest when written documents were very rare. However, a further more detailed study is foreseen to explore historical or archeoseismological data to confirm the identification of this youngest event.

Since the results of the first trench suggested strike-slip kinematics we excavated four additional fault-crossing trenches and two fault-parallel ones were excavated to trace the fault and offset features. Also 2D and 3D geophysical survey included electric resistivity tomography and ground penetration radar was carried out. The preliminary results of 3D trenching confirmed the M 6+ events during late Holocene, and together with the geophysical survey it revealed a complex geology and deformation probably as a result of right-lateral transpression during Late Quaternary (Fig. 35 and 36). Trenching survey revealed several fault strands with repeated movements and migrating activity towards the basin within a ~30 m-wide zone, which most probably form a single fault at the depth and which displaced Oligocene to Holocene sediments, as suggested by Blecha et al. (2019).

Event (bracket. units)	Age range	Faults involved	Expected minimum magnitude (used parameter)
Event 7 e1/f1	pre-Pliocene – post Oligocene	basin limit/flexure	
Event 6 f1/f2	pre-?500ka – Pliocene	F4	
Event 5 f1/f2	pre-?500ka – Pliocene	F3	M_W = 6.3 - 0.1 (MD-N)
Event 4 f3/g1	452 ka – 213 ka	F2	
Event 3 g1, f5/h1	3336 BC – 213 ka	F8, F6b	
Event 2 h1/h2	1134 BC – 192 BC	F1, F6a, F7a, F7b	M_W= 6.5 to 6.6 (MD-SS) M_W= 6.4 to 6.5 (MD-All)
Event 1 h2/h1	792 AD – 1020 AD	F1	M_W=6.5 (MD) M_W=6.1 to 6.5 (SRL– SS) M_W=6.1 to 6.4 (SRL-All)

Table 1: Summary of surface rupture events identified at both trench walls of Kopanina A and the assessed magnitude based on scaling relationships Magnitude versus Surface rupture length (SRL) and Magnitude vs Displacement (MD), calculated for strike slip (SS), normal fault (N) and All (Wells and Coppersmith 1994).See Štěpančíková et al. 2019.

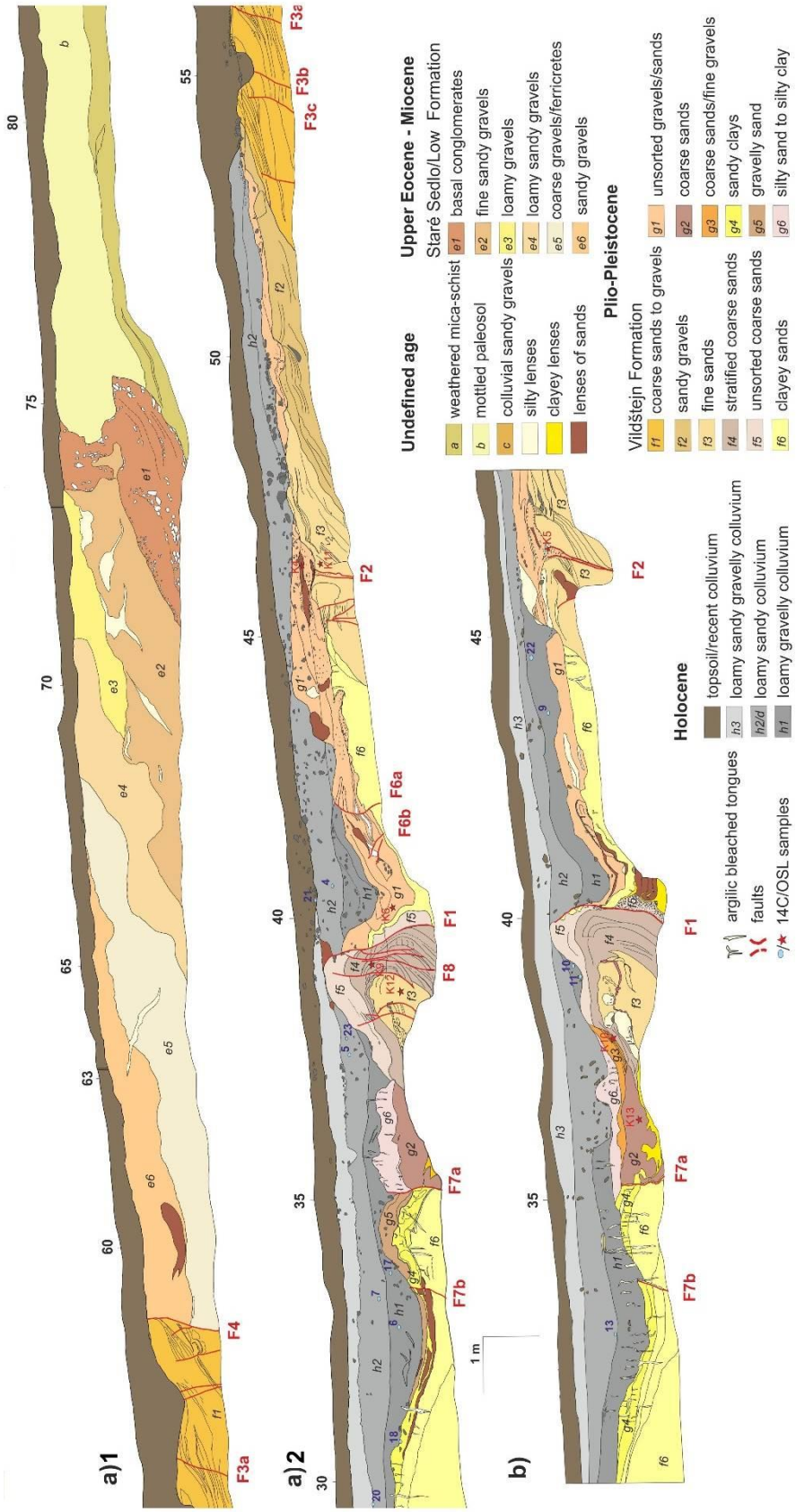

Fig. 34: Paleoseismological log of the Kopanina A trench with geological information. The footage of the trench is the same as in the ERT profile A. a1, a2 - divided log of SE-facing wall, b) - flipped NW-facing wall. Adapted from Štěpančíková et al. 2019.

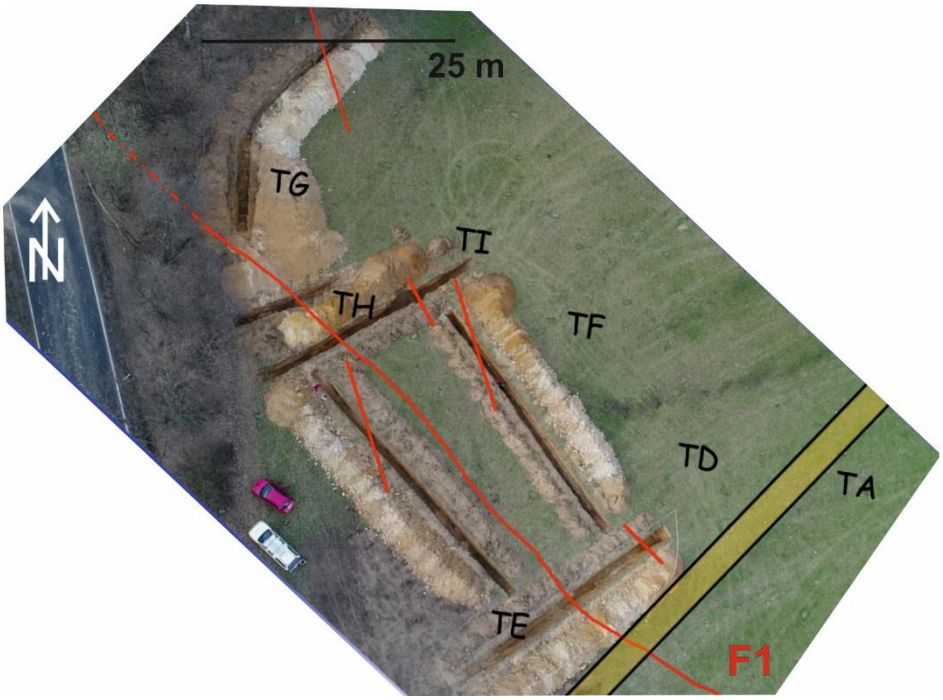

Fig. 35: The site Kopanina with trench position (Trench A, D, E, F, G, H, I) with faults (red line, F1- the main fault).

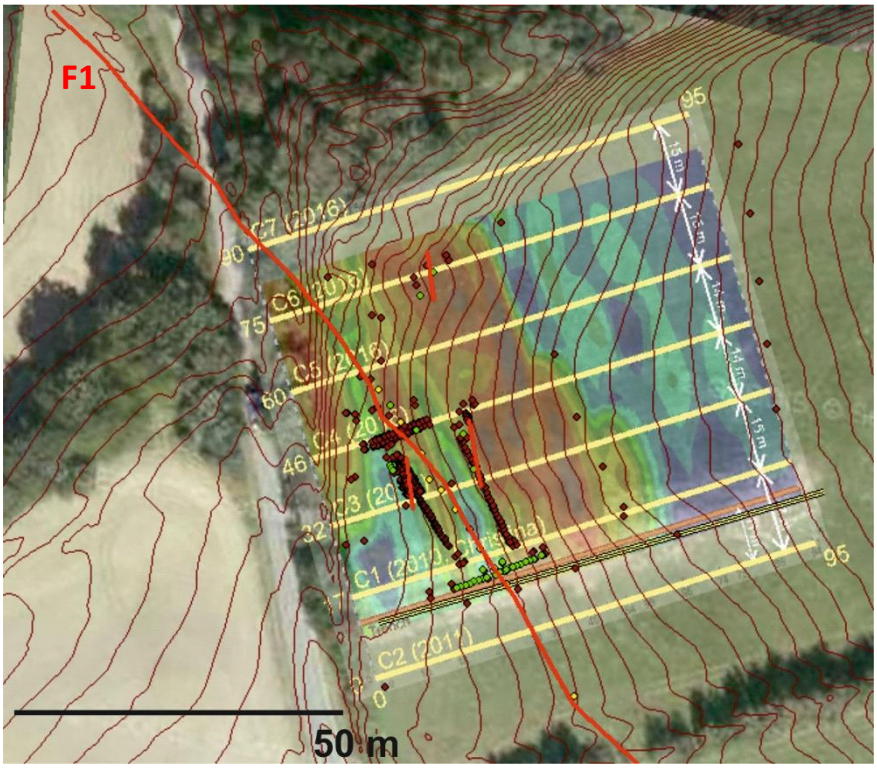

Fig. 36: Pseudo-3D electric resistivity tomography based on seven 2D ERT profiles - depth slice at around 3 m. Faults in red, F1 – the main fault.

4b) Kopanina: MULTI-ELECTRODE RESISTIVITY MEASUREMENTS (a field measurement method) & ELECTRICAL RESISTIVITY TOMOGRAPHY -ERT (a data processing & interpretation method)

(Tábořík, P.)

- ✓ uses artificial stationary electric field and Direct Current (DC)
- ✓ 2D/3D geophysical technique of shallow surveying, based on injecting of electric current by pair of electrodes C1, C2; and on measuring of electrical potential on pair of electrodes P1, P2.
- ✓ measurements are usually performed by using of a various number of multi-electrode cable sections and managed by device involving electronic control and switching units, voltmeter and ammeter (e.g. GF Instruments' Ares system or ABEM Terrameter etc.)

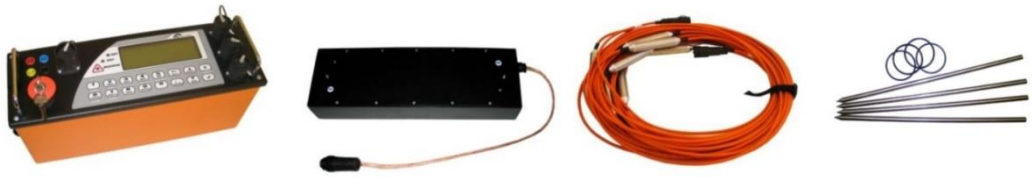

- ✓ a resolution in both horizontal and vertical direction, as well as penetration depth, are determined by electrode spacing and electrode array (configuration) used (with given geometry of a measurement)
- ✓ for the most used electrode configurations see the picture on right →

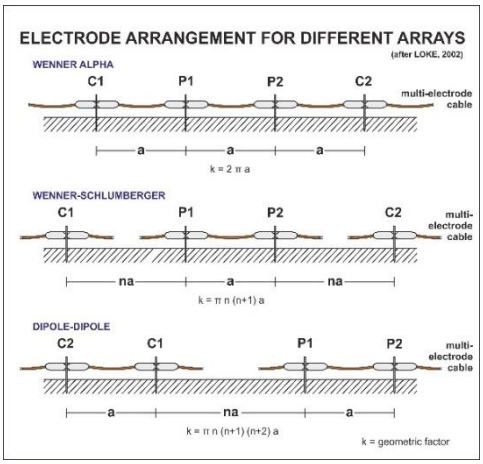

- ✓ using **modified Ohm's law**, apparent resistivity is determined from registered current and measured voltage:

$$\rho_a = \frac{2\pi}{\frac{1}{\overline{C_1P_1}} - \frac{1}{\overline{C_1P_2}} - \frac{1}{\overline{C_2P_1}} + \frac{1}{\overline{C_2P_2}}} \cdot \frac{U_{P_1P_2}}{I_{C_1C_2}} \quad \Rightarrow \quad \rho_a = k\frac{U}{I}$$

where $\overline{C_1P_1}, \overline{C_1P_2}, \overline{C_2P_1}, \overline{C_2P_2}$ are distances between electrodes (spacing), $\boldsymbol{\rho}_a$ [ohm.m] stands for apparent resistivity, **U** [mV] is voltage, **I** [mA] - current, **k** [m] - geometric factor

- ✓ measured ***apparent*** resistivity ($\boldsymbol{\rho}_a$) values are recalculated into ***„real"*** *(= modelled) resistivities* ($\boldsymbol{\rho}$) within the inversion process (e.g. in inversion software Res2Dinv) $\rho = k\frac{U}{I}$
- ✓ an interpretation is based on the final 2D/3D ERT model of a variating subsurface resistivity distribution, usually displayed by means of resistivity sections (= tomography)

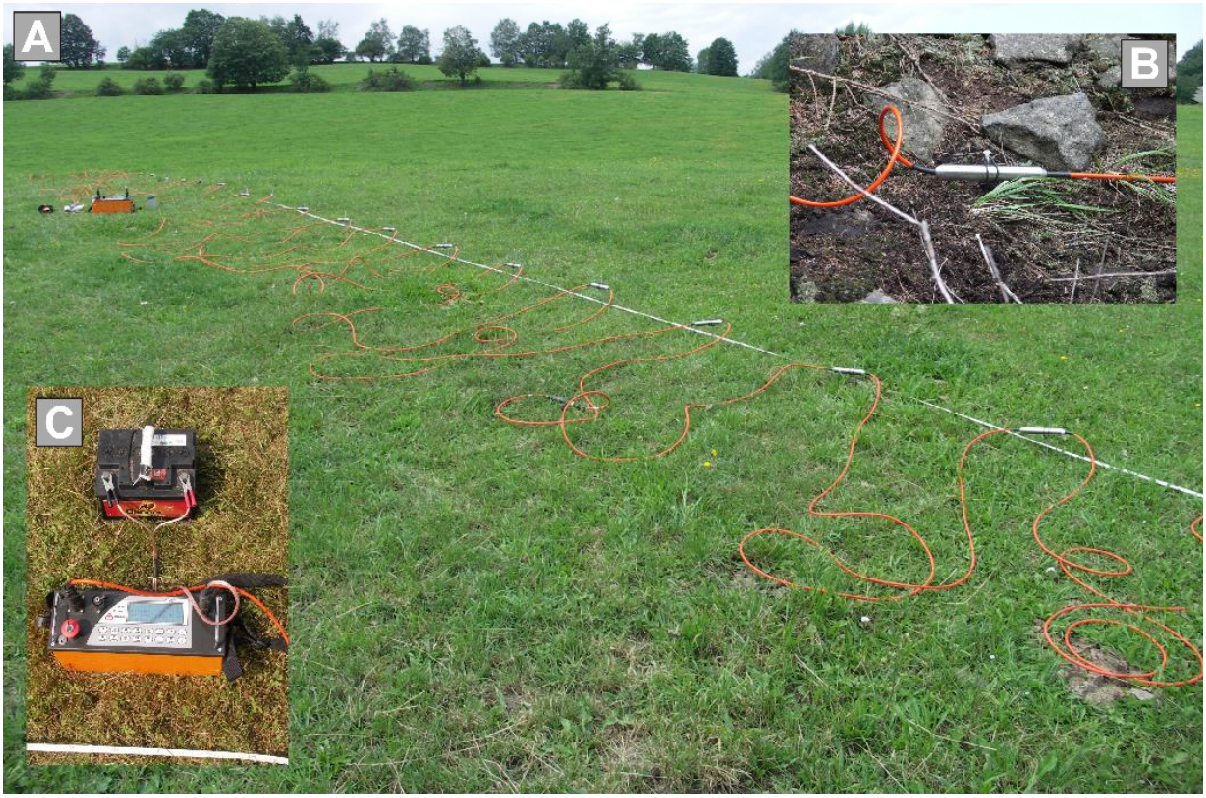

(A) multi-electrode cable sections laid along the profile; (B) grounded electrode in detail; (C) ARES - Automated Resistivity System with connected multi-electrode cables and power supply.

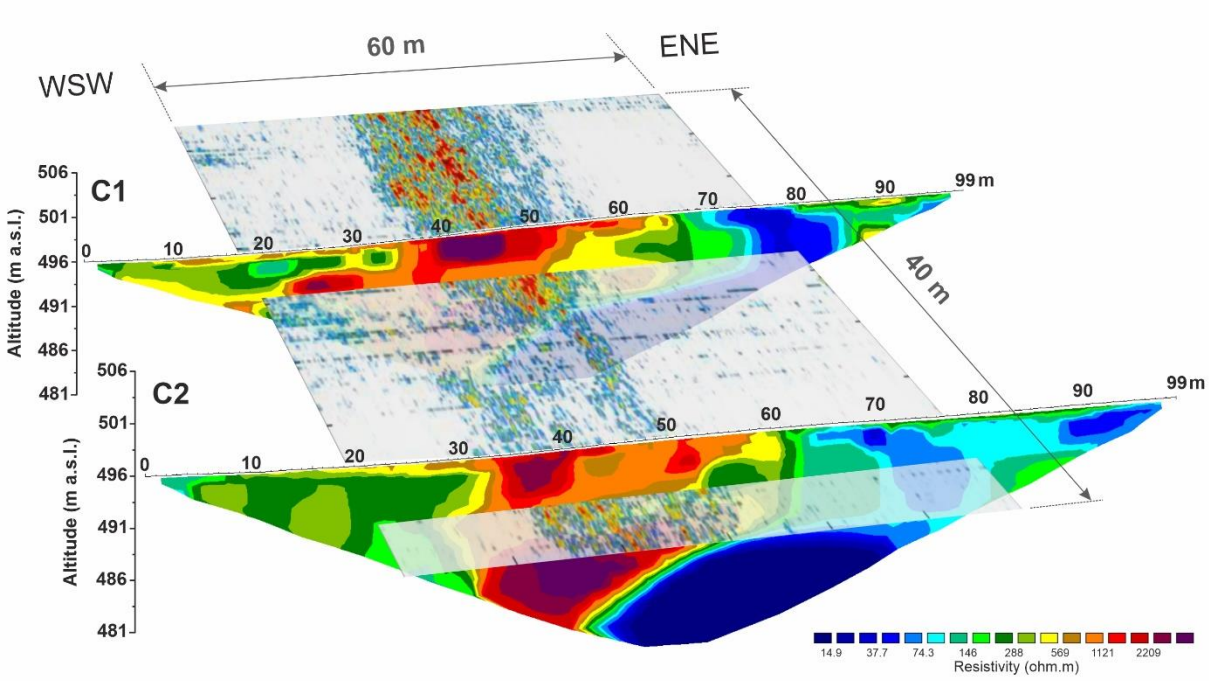

Intersection of the two ERT profiles and the GPR time slice corresponding to the depth of 5 m. Note the striking correlation between the high resistivity and high reflectivity of the material in the centre of the profiles. See Fig. 3 for the color scale of resistivities and Fig. 4 for the color scale of the GPR time slice. (see Fischer et al. 2012)

4b) Kopanina: DIPOLE ELECTROMAGNETIC PROFILLING (DEMP) (a field measurement method)

(Tábořík, P.)

- ✓ uses alternating current (AC) and electromagnetic (EM) field and belongs to the electromagnetic methods (sometimes called as "harmonic methods" due to the harmonic shape of the AC sinusoidal waveform)
- ✓ the method is based on a principle of EM induction when the primary field is induced at device transmitting coils, while the secondary EM field is induced in the subsurface environment as a response to the primary field. A receiver (also coil) records the intensity of the secondary field
- ✓ the DEMP method is thus contactless with no need of conductive coupling with the ground surface (and therefor is very fast and cheaper than other geoelectrical methods)
- ✓ **Theoretical basis of EM fields is defined by the <u>MAXWELL´S EQUATIONS</u>:**

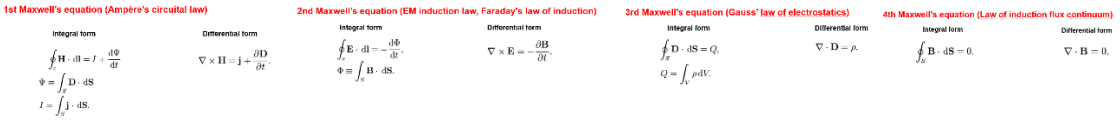

- ✓ pparent conductivity σ_a is the measured physical parameter, however it can be easily transfer to apparent resistivity ρ_a as its reciprocal value: $\rho_a = 1/\sigma_a$
- ✓ there are two ways how to penetrate deeper: (1) geometric approach (with an extending distance between the transmitting and receiving coils) and (2) frequency approach (with changing frequency for certain depths).
- ✓ Used CMD MiniExplorer and CMD Explorer are calibrated for following depths:

Exporer: 2.2 – 4.4 – 6.7 m ***MiniExplorer: 1.1 – 2.2 – 3.3 m***

- ✓ the measured data can be depicted as (A) 2D curves in several depths or 2D pseudosections of the variating apparent conductivity/resistivity along the profile, or (B) in 3D depth slices in case of areal measurements

(A) → **(B)**

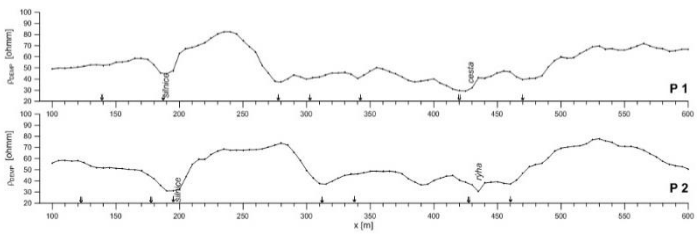

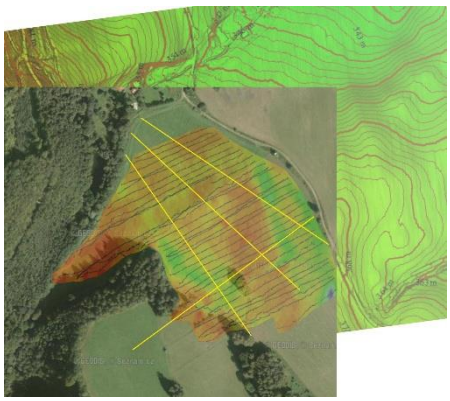

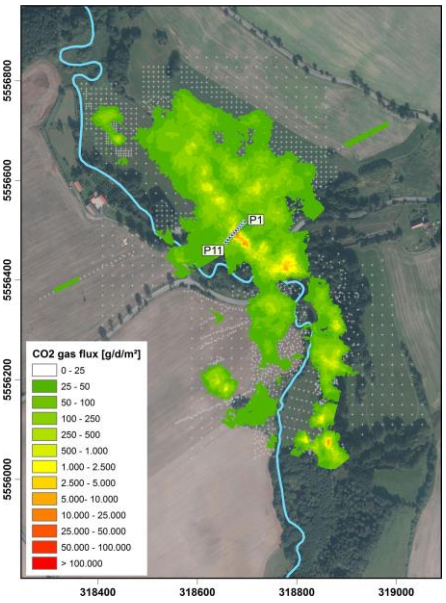

Fig. 37: Gas flux after interpolation of 3770 measuring points in the Hartoušov mofette field using trans-Gaussian kriging. White dots indicate the measuring position (from Nickschick et al., 2015)

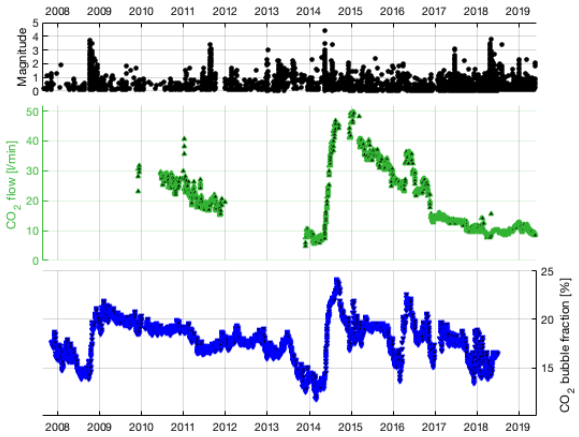

Fig. 38: Seismic activity in terms of local earthquake magnitudes (black), CO_2 flow (green) and fraction of gas bubbles in the water column (blue) in the F1 borehole in Hartoušov for the period 2008-2019.

Fig. 39: The largest mofette in the Bublák mofette field.

5) Hartoušov, Bublák

(Fischer, T.)

<u>Hartoušov mofette field</u>

The Hartoušov area came into the focus of interest of a multidisciplinary working group during the last years (see e.g. Nickschick et al., 2015, Fischer et al. 2017). It is located in the Plesná valley near the road bridge across the Plesná River. The Hartoušov mofette field is a typical example of CO_2 degassing in a dry form when the gas reaches the earth surface and escapes through openings in the ground which are dry or wet, filled by meteoric water.

The West Bohemia/Vogtland area is known for massive CO_2 degassing that occurs in the form of CO_2-rich mineral waters and wet and dry mofettes in several degassing fields. The total gas flow is concentrated in degassing centers of Cheb Basin, Mariánské Lázně and its eastern surroundings, and Karlovy Vary (Weinlich et al., 1999). These degassing centers are characterized by high gas flow, CO_2 concentrations of more than 99 vol.%, $\delta^{13}C$ values between ~–2 and ~–4‰, as well as high $^3He/^4He$ ratios up to 6 Ra (where Ra corresponds to the 3He/4He ratio of the atmosphere). Both these isotopic signatures point to the mantle origin of CO_2, which is the carrier phase for mantle-derived minor components (Bräuer et al., 2004; Weinlich et al., 1999).

The Hartoušov degassing area is located in the alluvial plain of the valley and is approx. 800 long and 300 m wide. It runs NNW-SSE. Since 2007 geophysical, geological as well as biological and geochemical studies have been carried out mainly in the southern part of the structure (reported by Kämpf et al. 2011). In this central area, which is slightly elevated, CO_2-degassing rates show the highest values and the content of chlorophyll of the plants is reduced (Pfanz & Sassmannshausen 2010). The plants are smaller than in the surroundings with lower root depth. Several slots occur with dead insects, birds and small animals.

Nickschick et al (2015) carried out detailed mappings of the CO_2 content in the soil and the CO_2 gas flux at the surface to define the extent of diffuse degassing structures. It turned out that measured gas fluxes at the surface are highly variable, both spatially and temporally (Fig. 37). An estimate of daily rate of 23 to 97 tons of CO2 discharge was obtained by statistical processing of measured data for the whole Hartoušov mofette field.

The diffuse degassing structure of Hartoušov represents a unique biosphere influenced by the CO_2. The biological investigations show more than 100 plant species with the dominance of grasses and sedges (Sassmannshausen 2010, Rennert et al. 2011). The distribution of the species correlates with the CO_2 content in the soil gas. Carbon isotopic investigations on the grass *Deschampsia cespotosia* indicate that in the degassing center the plants use up to 37 % of geogene CO_2 for covering their need of carbon (in Kämpf et al. 2011). The values of the CO_2 in the soil gas influence the composition of the individual species. It is remarkable that also springtails occur that are known only from Norway, the Arctic archipelagos, NE Siberia, and Middle Asia. The springtail *Folsomia mofettophila* (Schulz & Potapov 2011) was describted for the first time at the Hartoušov site. They belong to the springtail group of *Folsomia bisetosa* that are known from the circumpolar region.

The Hartoušov site also provides unique conditions for monitoring the CO_2 degassing in order to find its possible relations to the seismic activity. Since 2009 CO_2 flow monitoring has been carried out in a 29 m deep hydrological borehole tapping CO_2 saturated aquifer. During the 2014 M_L 4.5 seismic sequence a massive increase of CO_2 production was observed here followed by a long-term decay to original level; similar behavior was revealed by different

method during the 2008 M_L 3.3 seismic swarm in 2008 (Fig. 38). These coseismic anomalies were explained by the seismic valve model consisting of a fault rupture which breached through the sealing layer above CO_2 reservoir beneath the seismic zone. This was confirmed by numerical modelling of the diffusive flow of CO_2 through the upper crust from the rupture (Fischer et al., 2017). This way it was proved that carbon dioxide of magmatic origin passes on its way to the surface through seismically active faults and participates the seismogenic process.

Recently, Hartoušov became one of the sites of the Eger project (Drilling the Eger Rift: An observatory for study of fluid flow through the crust, non-volcanic, mid-crustal earthquake swarms and the deep biosphere) supported by the International Scientific Continental Drilling Program (ICDP). A field laboratory is being built here consisting of three boreholes at different levels aimed at underground monitoring of seismic activity, CO_2 degassing and its chemical composition and microbial activity. In past days drilling of the deepest borehole of 240 m depth was completed here.

Bublák mofette field

The Bublák mofette field occurs approx. 1.5 km north of the Hartoušov mofettes in a forest along the Plesná River. The highest $^3He/^4He$ ratios of the West Bohemian area reaching 6 Ra are documented here. It also includes the largest wet mofette in the area occurring in a pool more than 3 m wide (Fig. 39). A number of smaller mofettes occur in this area, including CO_2 bubbles in the Plesná River.

References:

Ambrož, V., 1958. Chebská pánev. Čas. Mineral. Geol., 3, 2, 178–190.

Blecha V., Fischer T., Tábořík P., Vilhem J., Klanica R., Valenta J., Štěpančíková P. (2018): Geophysical evidence of the Eastern Marginal fault of the Cheb Basin (Czech Republic). Studia Geophysica et Geodaetica, Volume 62, Issue 4, pp 660–680, DOI 10.1007/s11200-017-0452-9

Bucha, V., Horáček, J., Malkovský, M., 1990. Palaeomagnetic stratigraphy of the Tertiary of the Cheb Basin (W Bohemia). Věst. Ústř. Úst. geol 65 (5) pp. 267–278

Burda, J., Hartvich, F., Valenta, J., Smítka, V. and Rybář, J. (2012) Climate-induced landslide reactivation at the edge of the Most Basin (Czech Republic) - progress towards better landslide prediction., Nat. Hazards Earth Syst. Sci., 13, 361-374

Burda, J., Veselý, M., Řehoř, M., Vilímek, V. (2018): Reconstruction of a large runout landslide in the Krušené Hory Mts. (Czech Republic). Landslides, 15: 423 - 437

Bräuer, K., Kämpf, H., Niedermann, S. & Strauch, G. (2005): Evidence for ascending upper Mantle derived melt beneath the Cheb basin, central Europe. – Geophys. Res. Lett. 32, L08303, doi: 10.1029/2004GL022205.

Chlupáč I., Brzobohatý R., Kovanda J., Stráník Z.,2011. *Geologická minulost České republiky*. Academia.

Dèzes, P., Schmid, S.M., Ziegler, P.A., 2004. Evolution of the Cenozoic Rift System: interaction of the Alpine and Pyrenean orogens with their foreland lithosphere. Tectonophysics 389, 1–33.

Dostalík, M. a Malík, J. (2015): Dokumentace sesuvů v katastrálním území Poláky. Zpráva ČGS, ČGS-441/15/0638. SOG-441/224/2015, 1-10.

Fischer, T., P. Štěpančíková, M. Karousová, P. Tábořík, C. Flechsig, M. Gaballah, 2012. Imaging the Mariánské Lázně Fault (Czech Republic) by 3-D ground-penetrating radar and electric resistivity tomography. Stud. Geophys. Geod. 56

Fischer, T., Horálek, J., Hrubcová, P., Vavryčuk, V., Bräuer, K., Kämpf, H., 2014. Intra-continental earthquake swarms in West-Bohemia and Vogtland: a review, Tectonophysics 611, 1-27, doi: 10.1016/j.tecto.2013.11.001

Geissler, W. H., Kämpf, H., Bankwitz, P., Bankwitz, E., 2004. The Quaternary tephra-tuff deposit of Mýtina (southern rim of the western Eger Graben/Czech Republic): Indications for eruption and deformation processes (in German with summary in English). Z. Geol. Wiss. 32, 1, 31-54

Geissler, W.H., Kämpf, H., Kind, R., Klinge, K., Plenefisch, T., Horálek, J., Zedník, J., Nehybka, V., 2005. Seismic structure and location of a CO2 source in the upper mantle of the western Eger rift, Central Europe. Tectonics 24, TC5001. doi:0.10292004TC001672.

Hartvich, F. (2009): Reconstruction of the rockslide mechanics using various methods. Proceedings of the Conference „17. Tagung für Ingenieurgeologie“, Zittau, 6.-9. 5. 2009, Hochshule Zittau-Gorlitz, Germany, pp. 401-403

Hrubcová, P., Środa, P., Špičák, A., Guterch, A., Grad, M., Keller, G.R., Brückl, E., Thybo, H., 2005. Crustal and uppermost mantle structure of the Bohemian Massif based on CELEBRATION 2000 data. J. Geophys. Res. 110, B11305. doi: 10.1029/2004JB003080.

Hrubcová, P., Geissler, W.H., 2009. The Crust-Mantle Transition and the Moho beneath the Vogtland/West Bohemian Region in the Light of Different Seismic Methods. Stud. Geophys. Geod. 53, 275-294.

Hrubcová, P., Vavryčuk, V., Boušková, A., Horálek, J., 2013. Moho depth determination from waveforms of microearthquakes in the West Bohemia/Vogtland swarm area. J. Geophys., Res. 118, 1-17. doi:10.1029/2012JB009360.

Hrubcová, P., Geissler, W. H., Bräuer, K., Vavryčuk, V., Tomek, Č., Kämpf, H. 2017. Active magmatic underplating in western Eger Rift, Central Europe. Tectonics, 36. https://doi.org/10.1002/ 2017TC004710.

Kalvoda J, Vilímek V, Zeman A (1994) Earth's surface movements in the hazardous area of Jezeří kastle, Krušné hory Mts. GeoJournal 32(3):247–252

Kopecký L. (1971): Krušnohorsko-oharecká zóna, rýnský prolom a jejich význam pro hlubinnou stavbu. In: Výzkum hlubinné geologické stavby Československa, 157 – 185. MS Geofond. Praha.

Kopecký L. (1987): Mladý vulkanismus Českého masívu. Geologie a hydrometalurgie uranu, 3: 30 – 67 and 4: 3 – 44. VVU. Stráž pod Ralskem.

Kämpf, H., Peterek, A., Flechsig, C., Bräuer, K., Strauch, G. & Schunk, R. (2011): Junge Tektonik, Vulkanismus, aktive magmatische Prozesse und CO2-Geo-Bio-Wechselbeziehungen in der Schwarmbebenregion des westlichen Eger Rifts. – Exkursionsführer 21. Jahreshauptversammlung des Thüringischen Geologischen Vereins e. V. Marktredwitz 24. - 27.06.2011, 1-56, Jena.

Kárník, V., Michal, E., Molnár, A., 1957. Erdbebenkatalog der Tschechoslowakei bis zum Jahre 1956, Geofyzikální sborník, No. 69.

Klimeš, J., Rowberry, M.D., Blahůt, J., Briestenský, M., Hartvich, F., Košťák, B., Rybář, J., Stemberk, J., Štěpančíková, P. (2011): The monitoring of slow moving landslides and assessment of stabilisation measures using an optical-mechanical crack gauge. Landslides,. ol. 9, Issue 3, p. 407-415

Klimeš, J., Stemberk, J., Blahut, J., Krejčí, V., Krejčí, O., Hartvich, F. and Kycl, P. (2017): Challenges for landslide hazard and risk management in 'low-risk' regions, Czech Republic-landslide occurrences and related costs (IPL project no. 197). Vol. 14, Issue 2, p. 771-780

Košťák B (1969) A new device for in situ movement detection and measurement. Experimental Mechanics 9:374-379

Košťák B, Mrlina J, Stemberk J, Chán B (2011) Tectonic movements monitored in the Bohemian Massif. Journal of Geodynamics 52:34-44

Malkovský, M. (1979): Tektogeneze platformního pokryvu Českého masivu. Ústřední ústav geologický, Praha. 176 pp.

Malkovský, M., 1987. The Mesozoic and Tertiary basins of the Bohemian Massif and their evolution. Tectonophysics 137, 31–42.

Malkovský, M., 1995: Některé problémy chronostratigrafického členění českého masívu. Knihovnička ZPN, 16, 25-36.

Marek, J., Rybář, J, Chamra, S., Kudrna, Z., Vilímek, V., Forczek, I., Hartvich, F., Košťák, B., Stemberk J. and Schröfel, J. (2006): Evaluation of the geological phenomena threating historical heritage structures in the Czech Republic dominating the landscape scenery. Acta Research Reports, No. 15, Prague. P. 15-29.

Mrlina, J., 2000. Vertical displacements in the Nový Kostel seismoactive area. Studia geoph. et geod., 44, 336-345.

Mrlina, J., Špičák, A. and Skalský, L., 2003. Non-seismological indications of recent tectonic activity in the West Bohemia earthquake swarm region. J. Geodynamics, 35, 1-2, 221-234.

Mrlina, J., Kämpf, H., Geissler, W.H., van den Boogart, P. (2007): Assumed Quaternary maar structure at the Czech/German boundary between Mýtina and Neualbenreuth (western Eger Rift, Central Europe): geophysical, petrochemical and geochronological indications – Z. geol. Wiss., 35, 4- 5: 213-230.

Mrlina, J., Seidl, M., 2008. Relation of surface movements in west bohemia to earthquake swarms. Stud. Geophys. Geod. 52, 549-566.

Mrlina, J., Kämpf, H., Kroner, C., Mingram, J., Stebich, M., Brauer, A., Geissler, W.H., Kallmeyer, J., Matthes, H., Seidl, M., 2009. Discovery of the first Quaternary maar in the Bohemian Massif, Central Europe, based on combined geophysical and geological surveys. J. Volc. Geoth. Res. 182, 97-112. DOI: 10.1016/j.jvolgeores.2009.01.027.

Peterek, A., Reuther, C.D., Schunk, R., 2011. Neotectonic evolution of the Cheb Basin (Northwestern Bohemia, Czech Republic) and its implications for the late Pliocene to Recent crustal deformation in the western part of the Eger Rift. Z. Geol. Wiss. 39, 335-365.

Pešek, J. ed. 2014. Tertiary basins and lignite deposits of the Czech Republic. Czech Geological Survey, 283p.

Pitra, P., Burg, J. P., Guiraud, M, 1999: Late Variscan strike-slip tectonics between the Tepla-Barrandian and Moldanubian terranes (Czech Bohemian Massif): petrostructural evidence. Journal of the Geological Society, London, 156, 1003-1020.

Pfanz H., & Sassmannshausen, F. (2008): Geogenic CO2-Exhalations and Vegetation: Its possible use to predict volcanic eruptions, Geophys. Res. Abstr. 10, EUG2008-A-12108.

Rajdlová, H., 2001. Kvartérní paleoekologická analýza NPR Soos, master thesis, Charles University in Prague

Rennert, T., Eeustehues, K., Pfanz, H. & Totsche, K.U. (2011): Influence of geogenic CO2 on mineral and organic soil constituents on a mofette site in the NW Czech Republic, Eur. J. Soil Sci., akzeptiert, doi: 10.1111/j.1365-2389.2011.01355.x

Rojík, P., Fejfar, O., Dašková,J.,Kvaček, Z., Pešek, J., Sýkorová, I., Teodoridis, V. 2014. Cheb basin. In: Pešek, J. ed. Tertiary basins and lignite deposits of the Czech Republic. Czech Geological Survey, 143-161.

Rybář J (1981) Inženýrsko-geologické hodnocení stabilitních poměrů předpolí povrchových velkolomů při úpatí Krušných hor. Stabilitní řešení svahů a jejich zabezpečení, Sborník přednášek semináře, Most, pp, 76–93

Rybář, J. (1991): Untersuchung der Hangbewegungen in der ČSFR. – Felsbau, 9, 178-181. Verlag Glückauf GmbH. Essen

Sassmannshausen, F. (2010): Vegetationsökologische Charakterisierung terrestrischer Mofettenstandorte am Beispiel des westtschechischen Plesná-Tals, unv. Diss., Universität Duesburg- Essen.

Shebalin, N. V., Leydecker, G., Mokrushina, N. G., Tatevossian, R. E., Erteleva, O. O. and V. Yu. Vassiliev, 1998. Earthquake Catalogue for Central and Southeastern Europe 342 BC - 1990 AD. 247 p., 13 fig., 3 appendices; European Commission, Report No. ETNU CT 93 - 0087, Brussels.

Schulz, H.-J. & Potapov, M. (2010): A new species of Folsomia from mofette fields of the Northwest Czechia
(Collembola, Isotomidae), ZOOTAXA, 2253, 60-64.

Seifert, W., Kämpf, H., 1994. Ba-enrichment in phlogopite of a nephelinite from Bohemia. European Journal of Mineralogy 6, 497-502.

Spanilá, T., Kudrna, Z., John, V., Hartvich, F., and Chour, V. (2006): Assessment of factors and conditions influencing bank stability of future lakes. Acta Geodynamica et Geomaterialia, No. 4 (144), IRSM, Prague. P. 67-76.

Šibrava, V., Havlíček, P., 1980. Radiometric age of Plio-Pleistocene volcanic rocks of the Bohemian Massif. Věstník Ústředního Ústavu Geologického 55, 129-139.

Špičáková, L, Uličný, D, Koudelková, G, 2000. Tectonosedimentary evolution of the Cheb Basin (NW Bohemia, Czech Republic) between Late Oligocene and Pliocene: a preliminary note. Studia Geoph. Geod 44: 556–580.

Štěpančíková P., Fischer T., Stemberk J. jr., Nováková L., Hartvich F., Figueiredo M. P. (2019): Active tectonics in the Cheb basin: youngest documented Holocene surface faulting in central Europe? Geomorphology, 327, 15 February 2019, 472-488,

Teodoridis, V. , Bruch, A.A., Martinetto, E., Vassio, E., Kvaček, Z., Stuchlik, L., 2017. Plio-Pleistocene floras of the Vildštejn Formation in the Cheb Basin, Czech Republic – a review and a new paleoenvironmental evaluation – Palaeogeography, Palaeoclimatology, Palaeoecology, 467, 166-190.

Tyráček J., Minaříková D., Kočí A. (1987): Datování hradecké terasy Ohře.
Věst. Ústř. Úst. Geol., 62, 5, 279 – 289.

Ulrych, J., Lloyd, F. E., Balogh, K., 2003. Age relations and geochemical constraints of Cenozoic alkaline volcanic series in W Bohemia: A review. Geolines 15, 168-180.

Váně M. (1960): Debris and landslides at the foot of the krušné hory Mts. Čas Min Geol (2):174–177

Váně M. (1964): Tuchořice. In: Krutský N. (Ed.) Sborník k XV. Sjezdu Československé společnosti pro mineralogii a geologii s exkurzním průvodcem. Teplice. 264 pp.

Wagner, G.A., Gögen, K., Jonckhere, R., Wagner, I., Woda, C., 2002. Dating of Quaternary volcanoes Komorní hůrka (Kammerbühl) and Železná hůrka (Eisenbühl), Czech Republic, by TL, ESR, alpha-recoil and fission track chronometry. Z. Geol. Wiss. 30, 191-200.

Weinlich, F., Bräuer, K., Kämpf, H., Strauch, G., Tesař, J. & Weise, S. (1999): An active subcontinental mantle volatile system in the western Eger Rift, Central Europe: Gas flux, isotopic (He, C, and N) and compositional fingerprints. – Geochim. Cosmochim. Acta 63: 3652-3671.